arXiv:1407.6539v2 [cond-mat.supr-con] 22 Nov 2014

Emergent Spin Hall phase at a Lifshitz transition from competing orders

N. Mohanta,[1,*] S. Bandopadhyay,[2] S. Lal *,[2,†] and A. Taraphder[1,3]

[1] *Department of Physics, Indian Institute of Technology Kharagpur, W.B. 721302, India*
[2] *Department of Physical Sciences, Indian Institute of Science Education and Research Kolkata, W.B. 741252, India*
[3] *Centre for Theoretical Studies, Indian Institute of Technology Kharagpur, W.B. 721302, India*

The effects of competing orders, such as superconductivity and ferromagnetism, on a Fermi liquid are well established. A comprehensive understanding of such a competition in a metal whose Fermi surface has a non-trivial topology is yet to be achieved. Here, we address this question in a prototypical system: the 2D Rashba semimetal[1]. We show that dominant superconductivity interplays with Rashba spin orbit interactions (SOI) in forming a novel intrinsic anomalous Hall effect (AHE) with gapless edge states of Bogoliubov-de Gennes (BdG) quasiparticles. As in the case of itinerant ferromagnets[2], the intrinsic AHE arises from Berry curvature effects in the band structure. This phenomenon is robust even as subdominant ferromagnetism dramatically changes the nature of pairing symmetry[3,4]. An emergent spin Hall phase involving a change in Fermi-surface topology is found to accompany this Lifshitz quantum phase transition. We demonstrate the coexistence of the original and novel AHE in the presence of weak disorder. We offer a comparison of our results with experiments on the two dimensional electron gas at oxide heterointerfaces[5,6] as well as make some testable predictions.

AHE has been observed in wide variety of materials[2] such as complex oxide ferromagnets[7–10], ferromagnetic semiconductors[11], spinels[12,13], Heusler alloys[14,15], layered dichalcogenides[16] etc. The intrinsic mechanism for the AHE originates due to spin-orbit interaction (SOI) in parity-broken itinerant ferromagnets and is understood in terms of the Karplus-Luttinger semi-classical theory[17]. More recently, the intrinsic AHE has been explained as a topological mechanism: electrons at the Fermi surface can acquire a Berry phase from the existence of magnetic monopoles in momentum space arising from a non-trivial topology of electronic bands[11,18,19]. There are extrinsic contributions to the anomalous Hall conductivity (AHC), such as side-jump[20] or skew-scattering from impurities[21], which sometimes dominate over the intrinsic process[22].

A particularly simple model for the intrinsic AHE is the two-dimensional ferromagnetic Rashba model[23]. Here also, the AHE appears due to a Berry phase picked up at the avoided band-crossing induced by Rashba SOI (see Fig.(1(a) and (b))). The AHC σ_{xy} takes a finite value and is proportional to the Berry phase (in units of e^2/h) when there is a gap at the Fermi level at the avoided band-crossing point[24]. However, an additional singlet superconducting pairing gap at the Fermi level will suppress the magnetization induced gap responsible for stabilizing the AHE. This leads us to expect a clear suppression of the intrinsic AHE by the singlet superconductivity.

In this paper, we study the intrinsic AHE of BdG quasiparticles in two-dimensional s-wave superconductors with Rashba SOI and ferromagnetism based on a self-consistent mean-field solution of the pairing gap. The system is modeled by the following Hamiltonian

$$\mathcal{H} = \sum_{k,\sigma} \epsilon_k c^\dagger_{k\sigma} c_{k\sigma} + \alpha \sum_{k,\sigma,\sigma'} (\mathbf{g_k}\cdot\boldsymbol{\sigma})_{\sigma\sigma'} c^\dagger_{k\sigma} c_{k\sigma'} - m_z \sum_{k,\sigma,\sigma'} \boldsymbol{\sigma}^z_{\sigma\sigma'} c^\dagger_{k\sigma} c_{k\sigma'} + \sum_k (\Delta c^\dagger_{k\uparrow} c^\dagger_{-k\downarrow} + h.c.) \quad (1)$$

where $\epsilon_k = -2t(\cos k_x + \cos k_y) - \mu$ represents the dispersion of electrons, t the hopping parameter, μ the chemical potential, m_z the magnetization perpendicular to the two-dimensional plane, α the strength of Rashba SOI and $\mathbf{g_k} = (\sin k_y, -\sin k_x)$. $\Delta = -<c_{k\uparrow}c_{-k\downarrow}>$ is the superconducting pairing gap.

We briefly recall that for the case of a vanishing magnetization and s-wave superconductivity, the Rashba SOI leads to a cusp-like feature at the $(k_x = \pm\pi, k_y = \pm\pi)$ points in the electronic bands; the emergent electronic excitations around this cusp correspond to massless Dirac fermions[1] with a Berry phase $\gamma = \pi$ (see Fig. 1(a)). This gives rise to two edge currents in the system with opposite helicities, in turn giving a universal negative value of the intrinsic spin Hall conductivity (SHC) while the intrinsic AHC vanishes due to an exact cancellation. A finite superconducting order parameter will open a gap in the quasi-particle spectrum at the Fermi surface, leading to an avoided band-crossing at the cusp. This gives mass to the Dirac fermions, leading to a Berry phase for the BdG quasiparticles $\gamma < \pi$ (see Fig. 1(b)). It is expected that this Berry-phase contribution to the SHC remains finite in the presence of a superconducting order parameter[25–27]. The intra-band and inter-band pairing amplitudes in the two Rashba-split bands $\epsilon_\pm(\mathbf{k}) = \epsilon_k \pm \xi$, where $\xi = (\alpha^2|\mathbf{g_k}|^2 + m_z^2)^{1/2}$ are respectively $\Delta_\pm = (-\alpha|\Delta|/(2\xi))(\sin k_y \pm i \sin k_x)$ ($p_x \pm ip_y$-wave) and $\Delta_s = m_z|\Delta|/\xi$ (s-wave) (see supplementary information section A). As shown in Fig. 1(c), a stereographic projection of the energy contours on the (k_x, k_y) plane onto a sphere show that a finite superconducting order parameter turns the sphere into a ring torus.

Any finite magnetization in the system causes an imbalance in the spin populations of the BdG quasiparticles by introducing a Zeeman splitting between the helicity bands. Increasing the magnetization from zero also leads

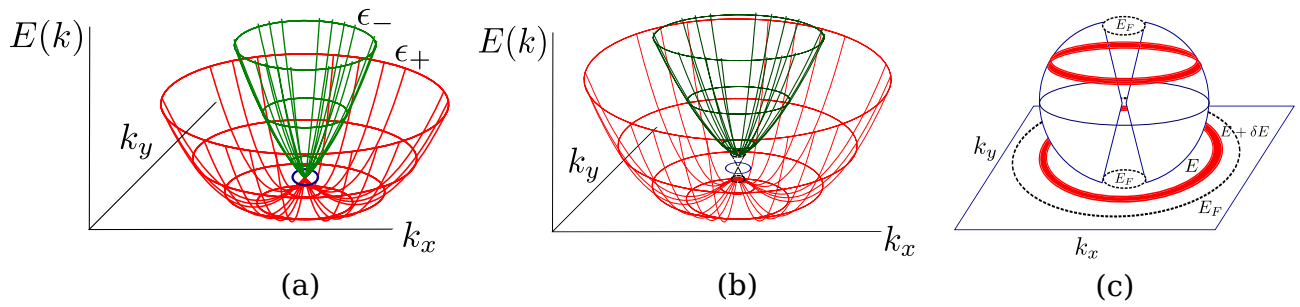

FIG. 1. (Color online) **The band structure for the 2D Rashba semimetal.** (a) A cusp-like feature connects the two bands ϵ_+ and ϵ_-, with a Dirac-like dispersion of the electrons. The blue circle displays a non-contractible loop around the Dirac point, with a non-trivial topology of the Fermi surface characterized by a Berry phase $\gamma = \pi$ (for the lower band). (b) The opening of a gap leads to a mass for the Dirac-like electronic excitations. The gap can arise due to a finite superconducting order parameter or magnetization. The black, dashed Dirac cone connecting the upper and lower bands signifies the gapless edge-states present in any finite system. These edge states are again surrounded by a non-contractible loop leading to a Berry phase $\gamma < \pi$, and make the system a Anomalous Hall insulator with topological properties. (c) A stereographic projection of the energy contours on the (k_x, k_y) plane onto a sphere touching the plane at its south pole. The black dashed line projects the Fermi energy onto a latitude near the North pole, while states with energies in the interval E to $E + \delta E$ (red band) are projected onto the northern hemisphere as shown. A finite superconducting order parameter connects the upper boundary with the south pole, making it topologically equivalent to a ring torus.

to a gradual closing of the avoided band-crossing at the $(k_x = 0, k_y = \pm\pi)$ and $(k_x = \pm\pi, k_y = 0)$ points near the Fermi level. This gives, in turn, an increase in the Berry curvature and thence the AHC from the neighbourhood of these four points in k-space. This can be seen by writing the Hamiltonian (1) in the Nambu-spin basis $\Psi = [\psi_k, \psi^\dagger_{-k}]$, where $\psi_k = [c_{k\uparrow}, c_{k\downarrow}]$, as

$$H(\mathbf{k}) = \begin{pmatrix} \epsilon_k - m_z\sigma_z + \alpha \mathbf{g_k}\cdot\boldsymbol{\sigma} & i\Delta\sigma_y \\ -i\Delta\sigma_y & -\epsilon_k + m_z\sigma_z + \alpha\mathbf{g_k}\cdot\boldsymbol{\sigma}^* \end{pmatrix} \quad (2)$$

From this, we obtain the quasi-particle spectrum

$$E(\mathbf{k})_\pm = \pm(\epsilon_k^2 + \xi^2 + \Delta^2 \pm 2\sqrt{\Delta^2 m_z^2 + \epsilon_k^2\xi^2})^{1/2}\ , \quad (3)$$

The quasi-particle spectrum for various values of the magnetization m_z is shown in Fig. 2.

When the chemical potential μ is inside the gap induced by the avoided band-crossing, the Berry curvature Ω and Berry phase γ picked up due to the lower band (with $p_x + ip_y$-wave pairing) is given by (see supplementary information section B for details)

$$\Omega = \frac{m_z^2\alpha^2|\Delta|^2\epsilon_+\cos k_x \cos k_y}{8\xi^4(\epsilon_+^2 + \Delta_+\Delta_-)^{3/2}}\ ,\ \gamma = \frac{1}{2\pi}\iint_{B.Z.} d^2\vec{k}\ \Omega(\vec{k}) \quad (4)$$

The AHC is obtained as $\sigma_{xy} = \frac{e^2}{2h}\gamma$[24,28]. The Berry phase contribution from the other BdG bands (whose pairing is $p_x - ip_y$-wave) is suppressed by the magnetization induced energy separation between the BdG bands of opposite helicity. In Fig. 3, the pairing amplitude Δ_+ and the Berry curvature Ω are shown in the first Brillouin zone (BZ) for various magnetization m_z. Δ_+ has nodal structure due to the Rashba SOI, while Ω shows finite value near the Fermi level. Further, the change in the topology of the band structure in the neighbourhood of the $(k_x = \pm\pi, k_y = 0)$ points is shown in the lower panel of Fig. 2: the effects of the competition between gaps induced by Δ and m_z are seen to change the topology of the BdG bands nearest to the superconducting gap via a Lifshitz transition[8]. A similar change happens at the $(k_x = 0, k_y = \pm\pi)$ points as well.

We stress that the AHE under consideration here is different from that obtained in the ferromagnetic Rashba model[23]: the gap at the Fermi level in the latter is opened by Zeeman splitting whereas in the former, the pairing gap serves the same purpose. Precisely at a critical value of the magnetization given by $m_z^* = \sqrt{\Delta^2 + \mu^2}$, where Δ is the superconducting order parameter and μ the chemical potential, we find massless Dirac fermions at the $(k_x = \pm\pi, k_y = 0)$ and $(k_x = 0, k_y = \pm\pi)$ points associated with an emergent SHE of the BdG quasiparticles. This can be seen in Fig. 2 with $m_z^*(\mu = 0) = \Delta$, as well as from the effective low-energy Hamiltonian in the neighbourhood of m_z^* (see supplementary information section C for details)

$$H_+(\mathbf{k}) = (v\sin k_y)\sigma_x + (v\sin k_x)\sigma_y + (m_z^* - m_z)\sigma_z \quad (5)$$

where the effective velocity of the emergent Dirac quasiparticles is given by $v = \alpha\ (1 - \frac{\mu^2}{m_z^{*2}})^{1/2}$. The mass of these quasiparticles is clearly seen to vanish at $m_z = m_z^*$. It is important to note that this effective low-energy subspace is formed out of two admixtures involving all four quasiparticle bands. The anomalous Hall and spin Hall conductivities computed for this system with a fixed $\Delta = 0.1$, $\mu = 0$ and with varying m_z is shown in Fig. 4(a). A finite SHC appearing sharply at the critical magnetisation m_z^* coincides with a vanishing AHC. This discontinuous behaviour of the AHC is a signature of a phase transition. The small value of the AHC for $m_z < m_z^*$ arises from the dominance of the s-wave superconductivity over ferromagnetism, while the sharp rise of the AHC in the regime $m_z > m_z^*$ signals the advent of a new SC order

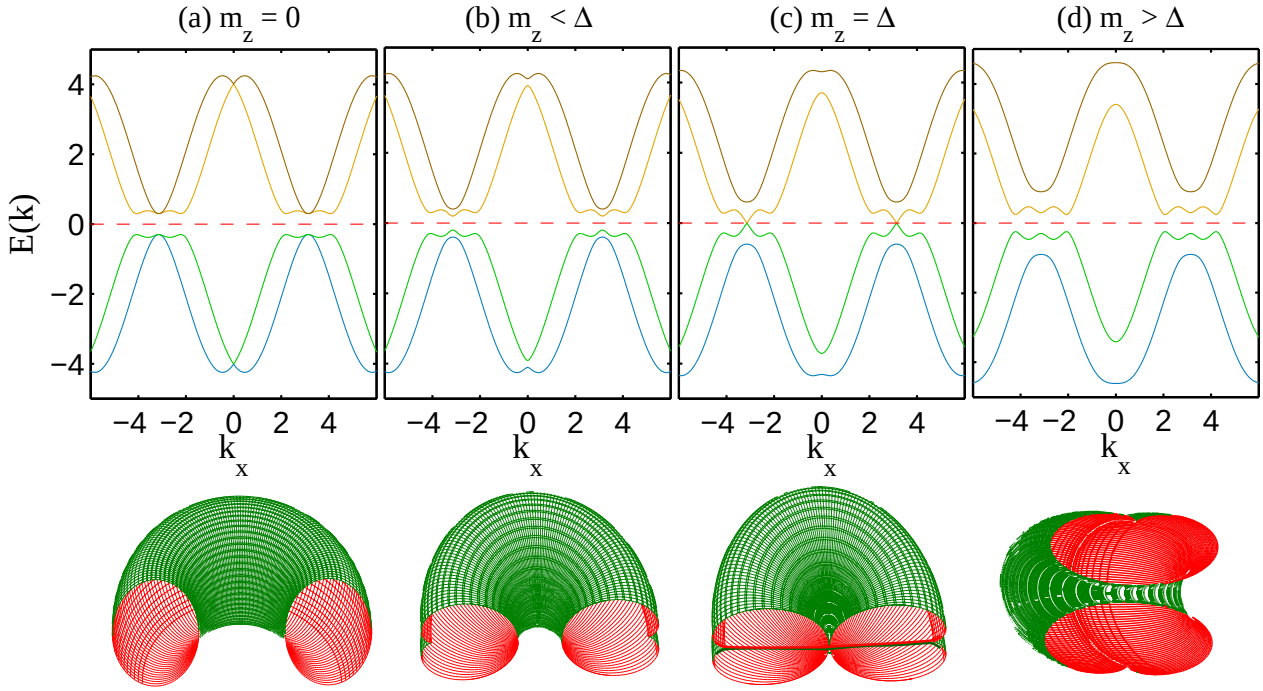

FIG. 2. (Color online) **The Bogoliubov- de Gennes (BdG) quasi-particle spectrum.** $E(k)$ as a function of k_x and with a fixed $k_y = 0$ for various values of the magnetization m_z with constant parameters $\mu = 0$, $\Delta = 0.3$, $\alpha = 1.0$ and $t = 1$. The avoided level-crossings near $(k_x = \pm\pi, k_y = 0)$ points at the Fermi-level give rise to finite Berry-phase γ leading to an AHE in the quasi-particle bands. Furthermore, as m_z increases, the quasi-particle excitation gap reduces and becomes zero at $m_z^* = \Delta = 0.3$ at $(k_x = \pm\pi, k_y = 0)$ in column (c). With further increase of m_z, a new excitation gap, proportional to Rashba SOI, opens up (column (d)) and the system undergoes a transition from topologically trivial to non-trivial superconductor. Figures in lower panel describe the topology of the two BdG bands nearest the superconducting gap in the neighbourhood of the $(k_x = \pm\pi, k_y = 0)$-points through the stereographic projection method described in Fig(1(c)). (a) As shown in Fig(1(c)), a finite superconducting order parameter turns the sphere into a ring torus by connecting its upper and lower boundaries. The effects of a competing incipient uniform magnetization can then be studied by considering its effects on the equatorial plane. (b) A finite magnetization gradually closes the gap defining the ring torus by uniformly pinching it on the equatorial plane. For a sub-dominant magnetization $m_z < m_z^*$, the inner hole of the ring torus is still dependent on the SC order parameter. (c) At $m_z = m_z^*$, the inner hole due to the superconductivity closes and the resulting topology is that of a Horn Torus which is pinched from two orthogonal directions. This change in the topology of the torus signals the quantum phase transition discussed above, coinciding with the emergent spin Hall phase. (d) For $m_z > m_z^*$, the topology is once again that of a ring torus, but whose inner hole is now dependent on the magnetization.

parameter discussed below. As shown in the mean-field phase diagram Fig. 4(b), the emergent SHE is concomitant with a quantum phase transition from normal superconductivity to topological superconductivity due to the dramatic change in pairing symmetry in the presence of Rashba SOI[3,4]. This is understood by noting that, upon tuning the magnetization in the regime $0 < m_z < m_z^*$, one of the helicity-bands is pushed away from the superconducting gap edge, and the inter-band s-wave pairing is thus strongly suppressed. For $m_z > m_z^*$, this leads the system into a phase taken to be a canonical example of topological superconductivity: a superconducting state with spinless $p_x + ip_y$-wave pairing belonging to the effective low-energy Hamiltonian

$$H_+(\mathbf{k}) = \begin{pmatrix} \epsilon_+ & \Delta_+ \\ \Delta_+^* & -\epsilon_+ \end{pmatrix} . \qquad (6)$$

Thus, beyond m_z^*, the quasi-particle gap is opened instead by the magnetization and Rashba SOI[30], leading to an intrinsic AHE which coexists with topological superconductivity. In this way, we find that the intervening SHE at the quantum critical point is correlated with the change in the momentum-space topology of the BdG quasiparticles shown in the lower panel of Fig. 2.

As tuning m_z through m_z^* leads to a crossing of bands at four points in momentum space ($(k_x, k_y) = (\pm\pi, 0)$ and $(0, \pm\pi)$), we can expect that the transition is first order in nature. As discussed by Volovik[1], the topological nature of this Lifshitz transition is further revealed by computing the Chern invariant $\tilde{N}_3$ related to the momentum space topology of the low-energy effective Dirac Hamiltonian, eq.(5) (see supplementary information section C for details). We find that $\tilde{N}_3$ changes from $-\frac{1}{2}$ to $\frac{1}{2}$ as m_z is tuned through m_z^* from below, with the massless Dirac point at $m_z = m_z^*$ possessing a Chern invariant $N_3 = \tilde{N}_3(m_z > m_z^*) - \tilde{N}_3(m_z < m_z^*) = 1$[1]. This corresponds to a singularity associated with a Dirac monopole in momentum space. Scattering an electron

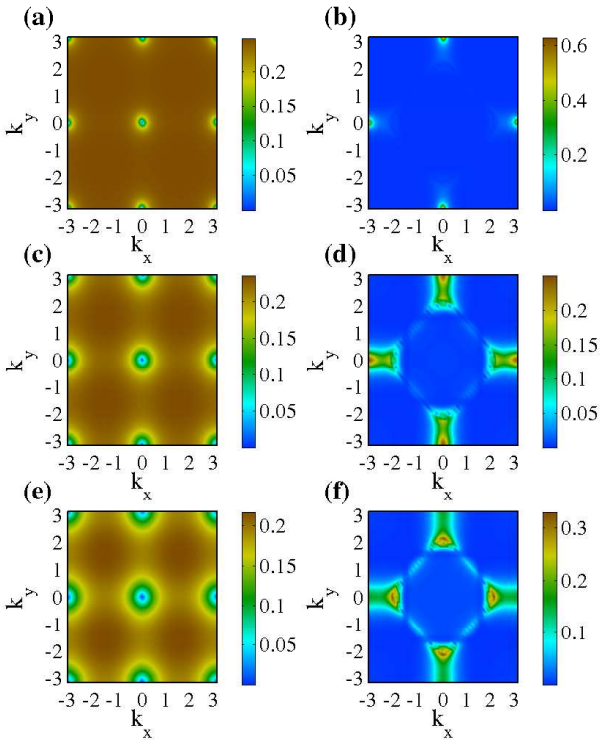

FIG. 3. (Color online) **Momentum-space plots of $|\Delta_+|$ and Ω.** The superconducting pairing amplitude $|\Delta_+|$ (left column) and the Berry curvature Ω (right column) for $m_z = 0.2$ in (a)-(b), $m_z = 0.5$ in (c)-(d) and $m_z = 0.8$ in (e)-(f). Other parameters: $\mu = 0$, $\Delta = 0.5$, $\alpha = 1.0$ and $t = 1$. Δ_+ has the nodal structure as the Rashba SOI. Ω takes finite values only at the avoided level-crossing at Fermi level in the quasi-particle spectrum. This is observed, for instance, at $(k_x = 0, k_y = \pm\pi)$ and $(k_x = \pm\pi, k_y = 0)$ in (d).

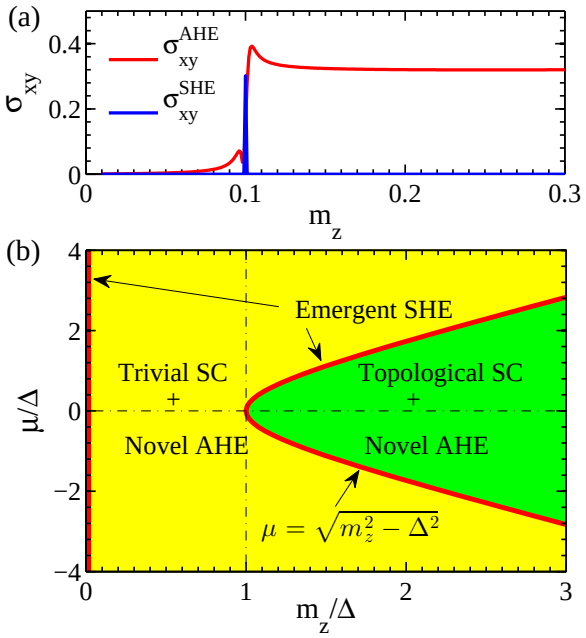

FIG. 4. (Color online) **Hall conductances and Phase diagram.** (a) The variation of the anomalous Hall conductivity σ_{xy}^{AHE} and the spin-Hall conductivity σ_{xy}^{SHE} with magnetization m_z for $\Delta = 0.1$ and $\mu = 0$. σ_{xy}^{SHE} shows a delta-function like peak only at $m_z = m_z^*$. (b) Phase diagram showing the appearance of different Hall phases and the superconductivity. It is evident that the emergent SHE will appear only at $m_z = 0$ and along the critical points defined by $\mu = \sqrt{{m_z}^2 - \Delta^2}$ line. On both the topologically trivial (yellow region) and non-trivial (green region) superconducting phases, the novel AHE is present.

from just below one of the Dirac points to just above the other can be described by a Berry phase-carrying instanton tunneling event that interpolates between the ground state of the system and an excited state that lies vanishingly close. The geometric phase associated with the massless Dirac electron observed at $m_z = m_z^*$ is π, while that with the instantons that tunnel between the ground state and the nearby excited state is $\pi/2$. As the Brillouin zone (i.e., the configuration space) connecting these two states is multiply connected, a destructive interference mechanism causes the tunnel splitting related to these instantons to vanish. This stabilizes the spin Hall ground state against the scattering of electrons between the Dirac cones. The spin Hall critical point is instead destabilised when the emergent time-reversal symmetry of the Dirac electrons is explicitly broken for $m_z \neq m_z^*$; this spoils the interference mechanism acting on the instantons, and generates a gap in the spectrum through a first order transition. The role played by topological excitations makes clear that this phase transition falls outside the Ginzburg-Landau-Wilson (GLW) paradigm. A field-theoretic description of this transition, the renormalisation group (RG) scaling relations and the $T = 0$ RG phase diagram are presented in the supplementary materials section D.

While the results presented above are robust for the case of a proximity-effect induced singlet superconducting pairing, we employ a self-consistent BdG formalism (see supplementary information section E) for the case when the pairing originates from an intrinsic superconducting instability of the 2D electronic system. In Fig. 5(a), (c) and (e) the variations of $|\Delta_+|$, $|\sigma_{xy}|$ and $|\sigma_{xy}^{2DEG}|$ (anomalous Hall conductivity for a ferromagnetic 2DEG with Rashba SOI) with various m_z and α are shown. Interestingly, both $|\Delta_+|$ and $|\sigma_{xy}|$ reveal non-monotonic behaviour with respect to increasing Rashba SOI strength α. This is due to the enhanced rate of spin-precession due to an increased α acts as a dephasing mechanism for superconductivity, thus reducing the superconducting pairing amplitude Δ. Also, this non-monotonic behaviour is the striking difference from the AHE in Ferromagnetic-2DEG with Rashba SOI (shown in Fig. 5(e)). A point-contact Andreev-tunneling spectroscopy can be used to probe this new type of AHE in Rashba-coupled superconductor. On the other hand, both $|\Delta_+|$ and $|\sigma_{xy}|$ are seen to decrease with increasing m_z as in FIG. 5(b) and (d). This is due to the fact that both the quantities depend explicitly on the pairing gap Δ, and a self-consistent treatment of Δ reveals that

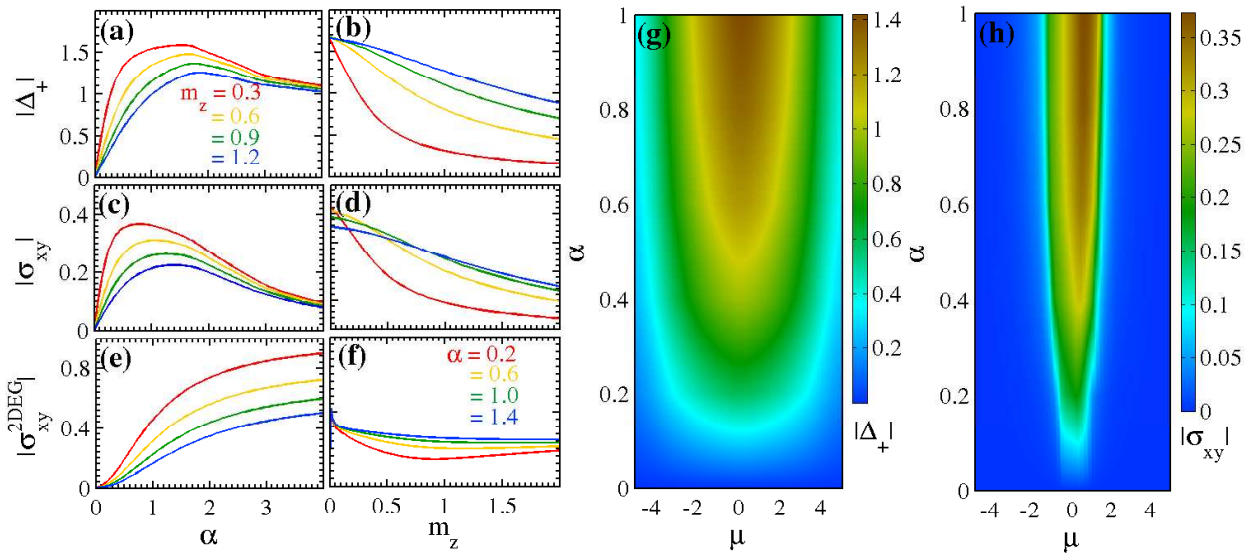

FIG. 5. (Color online) **Dependence of Pairing amplitude and Hall conductances on other parameters.** Figures (a)-(f) shows the variation of the pairing amplitude $|\Delta_+|$ and AHC $|\sigma_{xy}|$ and $|\sigma_{xy}|^{2DEG}$ (in units of $e^2/(2h)$) with magnetization m_z and Rashba SOI α with $\mu = 0$, $U = 2.0$ and $t = 1$. The non-monotonic feature of $|\sigma_{xy}|$ (Fig. (c)) distinguishes the novel AHE from the conventional AHE observed in ferromagnetic Rashba model without superconductivity. On the other hand, both $|\Delta_+|$ and AHC $|\sigma_{xy}|$ decays monotonically due to the explicit dependence in Δ which reduces with increasing m_z in the self-consistent calculation. Please note that, in Fig.(d), $|\sigma_{xy}|$ is valid except at $m_z = 0$ where the time-reversal symmetry is intact and we get an emergent SHE. Figures (g) and (h) are the plots of the pairing amplitude $|\Delta_+|$ and AHC $|\sigma_{xy}|$ (in units of $e^2/(2h)$) in the $\mu - \alpha$-plane for constant $U = 2.0$, $m_z = 0.5$ and $t = 1$. This shows that although superconductivity can be in a large filling-range, the AHE appears only within a narrow window of filling.

it decreases with an increasing m_z due to pair-breaking processes. The anomalous hall conductivity $|\sigma_{xy}^{2DEG}|$ decreases very slowly with m_z (shown in Fig. 5(f)) because with the increase of the gap at Fermi level, the Berry curvature reduces at very slow rate. The variations of the pairing gap Δ_+ and AHC σ_{xy} with the chemical potential μ are shown in Fig. 5(g)-(h). The pairing exists over a large filling range but the AHC is peaked only near the avoided level-crossings.

The nature of the variation of $|\Delta_+|$ with respect to the Rashba SOI (α) can shed light on the non-monotonic behaviour of superconductivity observed at $LaAlO_3/SrTiO_3$ interface[5,6]. In this Oxide interface, superconductivity ($T_c \simeq 200$ mK) is observed at very low-filling and the phase diagram is traced by varying the gate-voltage (V_g) which controls both the electron-concentration (n_{2D}) and the Rashba spin-orbit splitting (Δ_{so}). With increasing n_{2D}, the Curie temperature (T_c) should reveal a dome-shaped superconducting phase in the $n_{2D} - T_c$-space. However, the enhanced Δ_{so} serves as a pair-breaking agent and suppresses the superconductivity. With increasing V_g, both n_{2D} and Δ_{so} increase and the resulting competition between these two opposing effects leads to a non-monotonic behaviour.

Scattering from disorder, i.e, impurities which can be scalar potentials or even magnetic in nature, is a prominent feature of quantum transport. For instance, while a Bardeen-Cooper-Schrieffer (BCS) superconductor is robust against weak non-magnetic disorder [32], sufficiently strong disorder can drive the system to a non-superconducting state[33]. It is, therefore, interesting to analyse the nature of the AHE and its coexistence with the topological superconductivity in the disordered situation. The topological superconductivity is Rashba SOI-generated and non-local. Disorder can give rise to additional contributions to the AHC from side-jump and skew-scattering mechanisms[2]. However, it cannot degrade the contribution from the intrinsic Berry phase mechanism described above. This is because the Chern invariant $\tilde{N}_3$ is a topological property of a two-dimensional electronic system with broken time-reversal symmetry which was shown to be robust against electronic correlations and disorder scattering[34]. We choose, therefore, to focus instead on the effects of disorder on the competing orders and the associated phase transition discussed above.

We introduce non-magnetic disorder as a local shift in the chemical potential $H_{non-mag} = \sum_{i\sigma} V_d c^\dagger_{i\sigma} c_{i\sigma}$, where V_d is the random disorder potential which varies within $[-W, W]$, W being the maximum strength of the disorder. FIG. 6 (a) - (c) represents the real-space profile of the pairing gap $\Delta(r_i)$ and the magnetization $m(r_i)$ calculated via a self-consistent BdG formalism (see supplementary information section F). In the strongly disordered system, these two competing orders stay apart in spatially excluded regions[35]. It is, therefore, inferred that the AHE observed in ferromagnetic Rashba model resides in the ferromagnetic regions while the novel AHE exists in the superconducting islands. In this way, disorder enables the mesoscale phase coexistence[36] of the two types

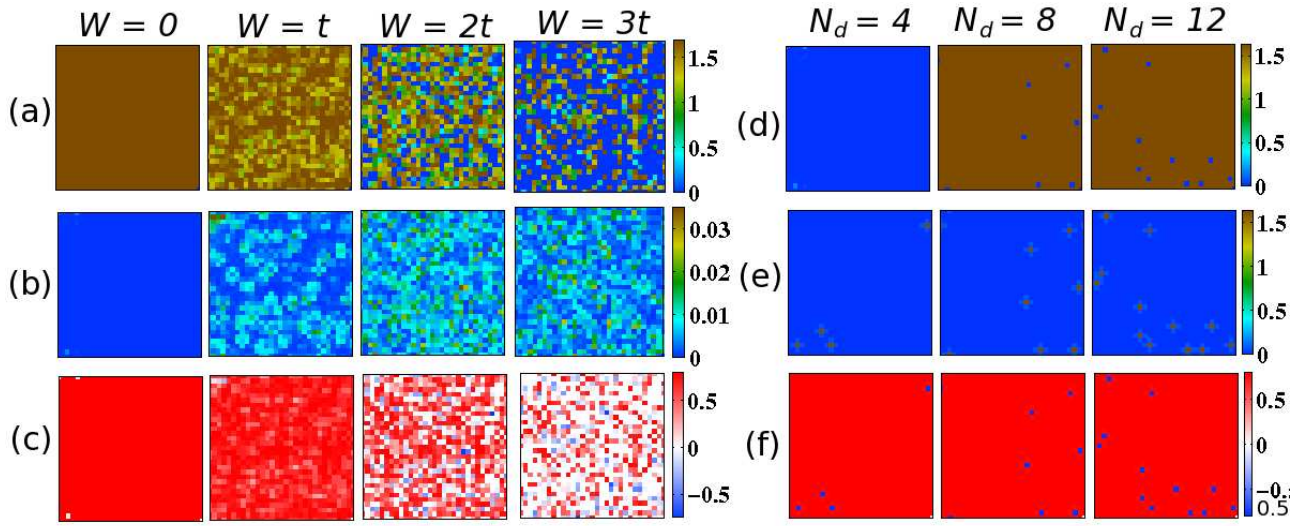

FIG. 6. (Color online) **Real-space effects of disorder.** The spatial distribution of the local pairing amplitude $|\Delta(r_i)|$ (top row) and magnetization (middle row) in 31×31 square lattice in the presence of disorder. The lowest row shows the spatial profile of the dominating order; red and blue colours represent regions of superconductivity and ferromagnetism. (a) - (c) The columns are for non-magnetic disorder strength $W = 0$, t , $2t$ and $3t$ (from left to right). The parameters used are $U = -1$, $m_z = 0.5$ and $\alpha = 0.8$. (d) - (f) The columns are for different number of magnetic impurities $N_d = 4$, 8 and 12 (from left to right). The parameters used are $U = -1$, $J_H = 1$ and $\alpha = 0.8$.

of AHE. Thus, the sharp phase boundary in the phase diagram Fig. 4(b) should be replaced with a phase separation region, with the transition belonging to the class of problems involving quantum percolation. The presence of massless Dirac electrons carrying π Berry phase was observed recently by Fernandes and Schmalian to be crucial for the appearance of complex critical exponents in the percolation transition in the 2D disordered Josephson junction array[37]; clearly, such a transition falls outside the GLW paradigm. The same can be expected for the transition in the present problem with disorder. Further, when the Rashba SOI and Zeeman field is large enough to convert the ordinary superconductivity into a topological one, the resulting topological superconductivity will be increasingly vulnerable to non-magnetic impurity scattering due to explicitly broken time-reversal symmetry[38]. Magnetic impurities, on the other hand, have detrimental effects on s-wave superconductors. At the mean-field level, the magnetic impurities can be described by the Hamiltonian $\hat{H}_{mag} = -J_H/2 \sum_{j,\sigma,\sigma'} \boldsymbol{\sigma}^z_{\sigma\sigma'} c^\dagger_{j\sigma} c_{j\sigma'}$, where j runs over N_d number of impurity sites, randomly located in the two-dimensional space (see supplementary information section G). As shown in FIG. 6 (d) - (f), superconductivity is totally destroyed at the impurity sites and we again have the spatial separation of superconductivity and ferromagnetism. As in the case of non-magnetic disorder, here also the two types of AHE coexist: the conventional AHE resides at the impurity sites and the novel AHE at the superconducting regions.

To summarize, we have proposed a novel AHE of BdG quasiparticles which arises from an interplay of singlet superconducting pairing and a finite perpendicular magnetization in presence of Rashba SOI. At a critical magnetization, an emergent spin Hall phase is found to coincide with a transition from normal to topological superconductivity. The quantum phase transition is shown to be driven by instanton excitations that change the topological nature of the ground state. At yet larger magnetization, the topological superconductivity coexists with the AHE. For the case when superconductivity is suppressed completely by magnetization, we expect a first order phase transition into an emergent intrinsic AHE phase of the ferromagnetic 2DEG Rashba model. We observed non-monotonic behaviour of the AHC with respect to the Rashba SOI strength due to the fact that at very large SOI, the enhanced spin-precession is pair-breaking for superconductivity. In this connection, we explain the non-monotonic feature of superconductivity observed at $LaAlO_3/SrTiO_3$ interface when gate-voltage is tuned. The non-monotonic dependence of the AHC on Rashba SOI in the presence of a superconducting order parameter can be easily distinguished from that obtained in its absence. The coexistence of superconductivity and the AHE is also expected to lead to a subtle interplay between Andreev reflection and Hall conductivity of edge-state BdG quasiparticles in several of these phases. Additionally, we have studied the effects of disorder in this model-system and found that both magnetic and non-magnetic disorder result in a coexistence of the novel AHE with the conventional AHE observed in ferromagnetic Rashba model. The scenario presented here can likely also be observed in thin film superconductors with

broken time-reversal or centro-inversion symmetries.

ACKNOWLEDGEMENT

N.M. acknowledges MHRD, India for support. S.L. gratefully acknowledges support from the DST, Govt. of India through a Ramanujan fellowship. S.B. and S.L. thank CTS, IIT-Kharagpur for hospitality while a part of the work was conducted. S.B. and S.L. thank Anirban Mukherjee for several discussions and invaluable help with visualizing the Fermi surface topology diagrams.

AUTHOR CONTRIBUTIONS

All authors contributed equally to the development of the model, its analysis as well as the writing of the main text and supplementary materials.

ADDITIONAL INFORMATION

The authors declare no competing financial interests. Supplementary information accompanies this paper. Correspondence and requests for materials should be addressed to S.L. and A. T.

* nmohanta@phy.iitkgp.ernet.in
† slal@iiserkol.ac.in

[1] Sinova, J. *et al.* Universal Intrinsic Spin Hall Effect. *Phys. Rev. Lett.* **92**, 126603 (2004).

[2] Nagaosa, N., Sinova, J., Onoda, S., MacDonald, A. H., and Ong, N. P., Anomalous Hall effect. *Rev. Mod. Phys.* **82**, 1539 (2010).

[3] Fujimoto, S. Topological order and non-Abelian statistics in noncentrosymmetric s-wave superconductors. *Phys. Rev. B* **77**, 220501 (2008).

[4] Zhang, C., Tewari, S., Lutchyn, R. M. and Das Sarma, S. $p_x + ip_y$ Superfluid from s-Wave Interactions of Fermionic Cold Atoms. *Phys. Rev. Lett.* **101**, 160401 (2008).

[5] Richter, C. *et al.* Interface superconductor with gap behaviour like a high-temperature superconductor. *Nature* **502**, 528 (2013), Letter.

[6] Caviglia, A. D. *et al.* Electric field control of the $LaAlO_3/SrTiO_3$ interface ground state. *Nature* **456**, 624 (2008).

[7] Allen, P. B. *et al.* Transport properties, thermodynamic properties, and electronic structure of SrRuO. *Phys. Rev. B* **53**, 4393 (1996).

[8] Kats, Y., Genish, I. ,Klein, L. Reiner, J. W. and Beasley, M. R. Testing the Berry phase model for extraordinary Hall effect in SrRuO. *Phys. Rev. B* **70**, 180407 (2004).

[9] Izumi, M. ,Nakazawa, K. , Bando, Y. ,Yoneda, Y. and Terauchi, H. Magnetotransport of $SrRuO_3$ Thin Film on $SrTiO_3$ (001). *J. Phys. Soc. Jpn.* **66**, 3893 (1997).

[10] Mathieu, R. *et al.* Scaling of the Anomalous Hall Effect in $Sr_{1-x}Ca_xRuO_3$. *Phys. Rev. Lett.* **93**, 016602 (2004).

[11] Jungwirth, T. , Niu, Q. and MacDonald, A. H. Anomalous Hall Effect in Ferromagnetic Semiconductors. *Phys. Rev. Lett.* **88**, 207208 (2002).

[12] Oda, K. *et al.* Unusual Anomalous Hall Resistivities of $CuCr_2S_4$, $Cu_{0.5}Zn_{0.5}Cr_2Se_4$ and Cr_3Te_4. *J. Phys. Soc. Jpn.* **70**, 2999 (2001).

[13] Lee, W.-L. , Watauchi, S. , Miller, V. L., Cava, R. J. and Ong, N. P. Dissipationless Anomalous Hall Current in the Ferromagnetic Spinel $CuCr_2Se_{4-x}Br_x$. *Science* **303**, 1647 (2004).

[14] Galanakis, I. , Dederichs, P. H. and Papanikolaou, N. Slater-Pauling behaviour and origin of the half-metallicity of the full-Heusler alloys. *Phys. Rev. B* **66**, 174429 (2002).

[15] Block, T. , Carey, M. J., Gurney, B. A. and Jepsen, O. Band-structure calculations of the half-metallic ferromagnetism and structural stability of full- and half-Heusler phases. *Phys. Rev. B* **70**, 205114 (2004).

[16] Checkelsky, J. G. , Lee, M. , Morosan, E. , Cava, R. J. and Ong, N. P. Anomalous Hall effect and magnetoresistance in the layered ferromagnet $Fe_{14}TaS_2$: The inelastic regime. *Phys. Rev. B* **77**, 014433 (2008).

[17] Karplus, R. and Luttinger, J. M. Hall Effect in Ferromagnetics. *Phys. Rev.* **95**, 1154 (1954).

[18] Fang, Z. *et al.* The Anomalous Hall Effect and Magnetic Monopoles in Momentum Space. *Science* **302**, 92 (2003).

[19] Onoda, M. and Nagaosa, N. Topological Nature of Anomalous Hall Effect in Ferromagnets. *J. Phys. Soc. Jpn.* **71**, 19 (2002).

[20] Berger, L. Side-Jump Mechanism for the Hall Effect of Ferromagnets. *Phys. Rev. B* **2**, 4559 (1970).

[21] Smit, J. The spontaneous hall effect in ferromagnetics: I. *Physica* **21**, 877 (1955).

[22] Onoda, S. , Sugimoto, N. and Nagaosa, N. Intrinsic Versus Extrinsic Anomalous Hall Effect in Ferromagnets. *Phys. Rev. Lett.* **97**, 126602 (2006).

[23] Bychkov, Y. A. and Rashba, E. I. Oscillatory effects and the magnetic susceptibility of carriers in inversion layers. *Journal of Physics C: Solid State Physics* **17**, 6039 (1984).

[24] Dugaev, V. K. , Bruno, P. , Taillefumier, M. , Canals, B. and Lacroix, C. Anomalous Hall effect in a two-dimensional electron gas with spin-orbit interaction. *Phys. Rev. B* **71**, 224423 (2005).

[25] Kontani, H. , Goryo, J. and Hirashima, D. S. Intrinsic Spin Hall Effect in the s-Wave Superconducting State: Analysis of the Rashba Model. *Phys. Rev. Lett.* **102**, 086602 (2009).

[26] Gradhand, M. and Annett, J. F. The Berry curvature of the Bogoliubov quasiparticle Bloch states in the unconventional superconductor Sr_2RuO_4. *J. Phys.: Condens. Matter.* **26**, 274205 (2014).

[27] Chung, S. B. and Roy, R. Hall conductivity in the normal and superconducting phases of the Rashba system with Zeeman field. arXiv:1407.3883

[28] Culcer, D. , MacDonald, A. H. and Niu, Q. Anomalous Hall effect in paramagnetic two-dimensional systems. *Phys. Rev. B* **68**, 045327 (2003).

[29] Lifshitz, I. M., Anomalies of electron characteristics of a metal in the high pressure region. *Sov. Phys. JETP* **11**, 1130-1135 (1960).

[30] Alicea, J. Majorana fermions in a tunable semiconductor device. *Phys. Rev. B* **81**, 125318 (2010).
[31] Volovik, G. E. *The Universe in a Helium Droplet* (Oxford Univ. Press, Oxford, 2003).
[32] Anderson, P. W. Theory of dirty superconductors. *Journal of Physics and Chemistry of Solids* **11**, 26 (1959).
[33] Dubi, Y. , Meir, Y. and Avishai, Y. Nature of the superconductor-insulator transition in disordered superconductors. *Nature* **449**, 876 (2007).
[34] Ishikawa, K. and Matsuyama, T. A microscopic theory of the quantum Hall effect. *Nuclear Phys. B* **280**, 523 (1987).
[35] Mohanta, N. and Taraphder, A. Phase segregation of superconductivity and ferromagnetism at the LaAlO 3 /SrTiO 3 interface. *J Phys: Condens. Matter* **26**, 025705 (2014); *ibid*, **26**, 215703 (2014).
[36] Dagotto, E. Complexity in strongly correlated electronic systems. *Science* **309**, 257 (2005).
[37] Fernandes, R. M. and Schmalian, J. Complex critical exponents for percolation transitions in Josephson-junction arrays, antiferromagnets, and interacting bosons. *Phys. Rev. Lett.* **106**, 067004 (2011).
[38] Potter, A. C. and Lee, P. A. Engineering a $p + ip$ superconductor: Comparison of topological insulator and Rashba spin-orbit-coupled materials. *Phys. Rev. B* **83**, 184520 (2011).

Supplementary Informations

A. Pairing symmetry in Rashba-split bands

The energy bands (consider Hamiltonian (1), in main text, without superconductivity) created by the Rashba SOI and magnetization are given by $\epsilon_\pm(\mathbf{k}) = \epsilon_k \pm \xi$, where $\xi = (\alpha^2|\mathbf{g_k}|^2 + m_z^2)^{1/2}$ and the corresponding eigenstates $[c_{k,+}, c_{k,-}]$ are obtained by the following transformation

$$\begin{pmatrix} c_{k\uparrow} \\ c_{k\downarrow} \end{pmatrix} = \frac{1}{\sqrt{2}} \begin{pmatrix} a_1 & b_1 e^{i\phi} \\ a_2 e^{-i\phi} & b_2 \end{pmatrix} \begin{pmatrix} c_{k,+} \\ c_{k,-} \end{pmatrix} \tag{S1}$$

where $\phi = \tan^{-1}(\sin k_x / \sin k_y)$, $a_1 a_2 = b_1 b_2 = -\alpha|\mathbf{g_k}|/(2\xi)$ and $a_1 b_2 - b_1 a_2 = m_z/\xi$. When written in the quasi-particle basis $[c_{k,+}, c_{k,-}]$, Hamiltonian (1), in main text, reduces to

$$\begin{aligned} \mathcal{H} = \sum_k [&\epsilon_+(\mathbf{k}) c^\dagger_{k,+} c_{k,+} + \epsilon_-(\mathbf{k}) c^\dagger_{k,-} c_{k,-} \\ &+ \Delta_\pm c^\dagger_{k,\pm} c^\dagger_{-k,\pm} + \Delta_s c^\dagger_{k,+} c^\dagger_{-k,-} + h.c.] \end{aligned} \tag{S2}$$

where $\Delta_\pm = (-\alpha|\Delta|/(2\xi))(\sin k_y \pm i \sin k_x)$ and $\Delta_s = m_z|\Delta|/\xi$ are, respectively, the intra-band and inter-band pairing amplitudes. Evidently, $\Delta_\pm$ has chiral p-wave pairing symmetry whereas Δ_s is of s-wave symmetry.

B. Calculation of Berry curvature of Bogoliubov-de Gennes bands

Any 2x2 traceless Hamiltonian can be written as

$$H = \begin{pmatrix} f_3 & f_1 - i f_2 \\ f_1 + i f_2 & -f_3 \end{pmatrix} = \sum_{i=1,2,3} f_i \sigma_i \ , \tag{S3}$$

where the σ_i are the three Pauli matrices. Now, the relation for the Berry curvature Ω can be written in the following form

$$\Omega = -\Im \frac{\langle + | \nabla_k H | - \rangle \times \langle - | \nabla_k H | + \rangle}{4E^2} \ , \tag{S4}$$

where E is the modulus of the eigenvalue of the Hamiltonian and $|\pm\rangle$ are the normalized eigenstates. In our case, $E = \sqrt{f_1^2 + f_2^2 + f_3^2}$, $\nabla_k H = \sigma_i \nabla_k f_i$ and

$$|\pm\rangle = \frac{1}{\sqrt{2E(E - f_3)}} \begin{pmatrix} f_1 - i f_2 \\ \pm E - f_3 \end{pmatrix} \ . \tag{S5}$$

As, $\nabla_k f_i$ is a number, we have to calculate the following matrix elements

$$\begin{aligned} &\langle - | \sigma_1 | + \rangle = \frac{-f_1 f_3 + i E f_2}{E(E^2 - f_3^2)} \ , \ \langle - | \sigma_2 | + \rangle = \frac{-f_2 f_3 - i E f_1}{E(E^2 - f_3^2)} \ , \\ &\langle - | \sigma_2 | + \rangle = \frac{\sqrt{E^2 - f_3^2}}{E} \ . \end{aligned} \tag{S6}$$

Now, the formula for Berry curvature Ω will be

$$\Omega = -\Im \frac{(\langle + | \sigma_i | - \rangle \nabla_k f_i) \times (\langle - | \sigma_i | + \rangle \nabla_k f_i)}{4E^2} \ . \tag{S7}$$

First consider the term, $\nabla_k f_1 \times \nabla_k f_2$ with a coefficient c_3

$$\begin{aligned} c_3 &= \Im(\langle + | \sigma_1 | - \rangle \langle - | \sigma_2 | + \rangle - \langle + | \sigma_2 | - \rangle \langle - | \sigma_1 | + \rangle) \\ &= \frac{2E f_3 (f_1^2 + f_2^2)}{E^2(E^2 - f_3^2)} = \frac{2 f_3}{E} \ . \end{aligned} \tag{S8}$$

Now, using the rotational symmetry of the σ matrices we get

$$\Omega = -\frac{f_3(\nabla_k f_1 \times \nabla_k f_2) + f_2(\nabla_k f_3 \times \nabla_k f_1) + f_1(\nabla_k f_2 \times \nabla_k f_3)}{2E^3} \tag{S9}$$

Now, the chiral bands in the proximity of the Fermi level are the + bands, whose 2×2 Hamiltonian is given by

$$H_1 = \begin{pmatrix} \epsilon_+ & \Delta_+ \\ \Delta_+^* & -\epsilon_+ \end{pmatrix} \quad \text{for basis, } (c^\dagger_{k+}, c_{-k+}) \ , \tag{S10}$$

where $\epsilon_+ = -2t(\cos k_x + \cos k_y) - \mu + \xi$, $\xi = \sqrt{\alpha^2(\sin^2 k_x + \sin^2 k_y) + m_z^2}$, $\Delta_+ = -\frac{\alpha|\Delta|}{2\xi}(\sin k_y + i \sin k_x)$, with α being the Rashba SOI strength,m_z is the magnetisation, Δ is the superconducting pairing gap, μ is the chemical potential and t the hopping parameter. Mapping onto the general form of the 2×2 matrix form given above in equation (S3), the Berry curvature about the z-axis in spin space can be calculated from the relation

$$\Omega = \frac{-f_3(\partial_{k_y} f_1 \partial_{k_x} f_2 - \partial_{k_y} f_2 \partial_{k_x} f_1)}{2E^3} \tag{S11}$$

where $f_1 = \mathrm{Re}(\Delta_+) = -\frac{\alpha|\Delta| \sin k_y}{2\sqrt{\alpha^2(\sin^2 k_x + \sin^2 k_y) + m_z^2}}$,
$f_2 = \mathrm{Im}(\Delta_+) \equiv \Delta_- = -\frac{\alpha|\Delta| \sin k_x}{2\sqrt{\alpha^2(\sin^2 k_x + \sin^2 k_y) + m_z^2}}$,
$f_3 = \epsilon_+$ and $E = \sqrt{f_1^2 + f_2^2 + f_3^2} = \sqrt{\epsilon_+^2 + \Delta_+ \Delta_-}$. We can now compute the elements needed for the calculation

of the Berry curvature about the z-axis

$$\partial_{k_y} f_1 = -\frac{\alpha|\Delta|\cos k_y}{2\sqrt{\alpha^2(\sin^2 k_x + \sin^2 k_y) + m_z^2}} + \frac{\alpha^3|\Delta|\sin^2 k_y \cos k_y}{2(\sqrt{\alpha^2(\sin^2 k_x + \sin^2 k_y) + m_z^2})^3} \quad \text{(S12)}$$

$$\partial_{k_x} f_2 = -\frac{\alpha|\Delta|\cos k_x}{2\sqrt{\alpha^2(\sin^2 k_x + \sin^2 k_y) + m_z^2}} + \frac{\alpha^3|\Delta|\sin^2 k_x \cos k_x}{2(\sqrt{\alpha^2(\sin^2 k_x + \sin^2 k_y) + m_z^2})^3} \quad \text{(S13)}$$

$$\partial_{k_x} f_1 = \frac{\alpha^3|\Delta|\sin k_y \sin k_x \cos k_x}{2(\sqrt{\alpha^2(\sin^2 k_x + \sin^2 k_y) + m_z^2})^3} \quad \text{(S14)}$$

$$\partial_{k_y} f_2 = \frac{\alpha^3|\Delta|\sin k_y \sin k_x \cos k_x}{2(\sqrt{\alpha^2(\sin^2 k_x + \sin^2 k_y) + m_z^2})^3} . \quad \text{(S15)}$$

From here, we compute

$$\partial_{k_y} f_1 \partial_{k_x} f_2 = \quad \text{(S16)}$$
$$\frac{\alpha^6|\Delta|^2 \sin^2 k_x \sin^2 k_y \cos k_x \cos k_y}{4(\alpha^2(\sin^2 k_x + \sin^2 k_y) + m_z^2)^3} + \frac{\alpha^2|\Delta|^2 \cos k_x \cos k_y}{4(\alpha^2(\sin^2 k_x + \sin^2 k_y) + m_z^2)} \frac{\alpha^4|\Delta|^2(\sin^2 k_x \cos k_x \cos k_y + sin^2 k_y \cos k_x \cos k_y)}{4(\alpha^2(\sin^2 k_x + \sin^2 k_y) + m_z^2)^2} \quad \text{(S17)}$$

$$\partial_{k_y} f_2 \partial_{k_x} f_1 = \frac{\alpha^6|\Delta|^2 \sin^2 k_x \sin^2 k_y \cos k_x \cos k_y}{4(\alpha^2(\sin^2 k_x + \sin^2 k_y) + m_z^2)^3} \quad \text{(S18)}$$

$$\partial_{k_y} f_1 \partial_{k_x} f_2 - \partial_{k_x} f_1 \partial_{k_y} f_2 = \frac{\alpha^2|\Delta|^2 m_z^2 \cos k_x \cos k_y}{4(\alpha^2(\sin^2 k_x + \sin^2 k_y) + m_z^2)^2} . \quad \text{(S19)}$$

We can now finally compute the Berry curvature Ω as

$$\Omega = (\partial_{k_y} f_1 \partial_{k_x} f_2 - \partial_{k_y} f_2 \partial_{k_x} f_1) \cdot f_3/(2E^3) = \frac{\alpha^2|\Delta|^2 m_z^2 \cos k_x \cos k_y}{4(\alpha^2(\sin^2 k_x + \sin^2 k_y) + m_z^2)^2} \frac{\epsilon_+}{2(\epsilon_+^2 + \Delta_+\Delta_-)^{\frac{3}{2}}} = \frac{m_z^2 \alpha^2|\Delta|^2 \epsilon_+ \cos k_x \cos k_y}{8\xi^4(\epsilon_+^2 + \Delta_+\Delta_-)^{\frac{3}{2}}} . \quad \text{(S20)}$$

This is the result presented in the main text.

C. Derivation of effective low-energy Hamiltonian and calculation of the effective velocity of the emergent Dirac quasi-particles

A Rashba Hamiltonian in the spin $(\uparrow,\downarrow)$ basis

$$H_R = \begin{pmatrix} \epsilon_k - m_z & \alpha g_k \\ \alpha g_k^* & \epsilon_k + m_z \end{pmatrix} \quad \text{(S21)}$$

can be diagonalized in the chiral basis $(+-)$

$$H_R = \begin{pmatrix} \epsilon_+ & 0 \\ 0 & \epsilon_- \end{pmatrix} , \quad \text{(S22)}$$

where $\epsilon_\pm = \epsilon_k \pm \sqrt{\alpha^2|g_k|^2 + m_z^2}$ & $g_k = \sin k_y + i \sin k_x$. Upon including finite triplet pairing $\Delta_\pm$ and singlet pairing Δ_s order parameters, the Rashba Hamiltonian can be written in the Nambu basis, $(c_{k+}, c_{k-}, c_{-k-}^\dagger, c_{-k+}^\dagger)^T$, as

$$H = \begin{pmatrix} \epsilon_+ & 0 & \Delta_s & \Delta_+ \\ 0 & \epsilon_- & \Delta_- & \Delta_s \\ \Delta_s & \Delta_-^* & -\epsilon_- & 0 \\ \Delta_+^* & \Delta_s & 0 & -\epsilon_+ \end{pmatrix} , \quad \text{(S23)}$$

where the triplet pairing $\Delta_\pm = -\frac{\alpha|\Delta|}{2\sqrt{\alpha^2|g_k|^2+m_z^2}}(\sin k_y \pm i \sin k_x)$ and the singlet pairing is $\Delta_s = \frac{m_z|\Delta|}{2\sqrt{\alpha^2|g_k|^2+m_z^2}}$. This Hamiltonian can easily be projected to a 2x2 Hamiltonian in two cases: (i) triplet pairing is quite small in compared to the singlet pairing ($\Delta_\pm << \Delta_s$) and (ii) the triplet pairing is much larger than the singlet pairing ($\Delta_\pm >> \Delta_s$). For the first case, the Rashba spin-orbit coupling α is very small and leads to small band mixing. This is not the case of interest in the present study, and henceforth, we will focus on the case (ii). Here, bands with similar chirality will undergo mixing. We will consider this case in four different situations, as discussed below.

Case I: $m_z = 0$

Here, Δ_s goes to zero. The Hamiltonian then gets separated in two subspaces of different chirality

$$H_1 = \begin{pmatrix} \epsilon_+ & \Delta_+ \\ \Delta_+^* & -\epsilon_+ \end{pmatrix} \text{ for basis, } (c_{k+}^\dagger, c_{-k+}) , \quad \text{(S24)}$$

and

$$H_2 = \begin{pmatrix} \epsilon_- & \Delta_- \\ \Delta_-^* & -\epsilon_- \end{pmatrix} \text{ for basis, } (c_{k-}^\dagger, c_{-k-}) . \quad \text{(S25)}$$

Each of H_1 and H_2 will give rise to their own topological invariant, but have opposite chirality. Hence, the charge currents arising from the two chiralities will ameliorate one another. In fact, at the $(k_x, k_y) = (\pm\pi, 0)$ and $(0, \pm\pi)$ points, the charge current contributions from H_1 and H_2 are identical in magnitude but opposite in sign; they will thus cancel one another. Thus, instead of an anomalous charge Hall conductivity, we find a spin Hall conductivity at these points in momentum-space.

Case II: $m_z << \alpha, \Delta$

A small magnetization m_z favours one of the chiralities and diminish transport effects due to the other. Further, the s-wave SC order parameter Δ_s causes mixing between the + and − chiralities and leads to a suppression of the anomalous Hall conductivity (AHC) in this regime.

Case III: $\alpha >> m_z >> \Delta$

As m_z crosses the strength of Δ, the system enters into the topological superconductor phase and only one chirality remains with the Hamiltonian given by eq.(S24).

We can see from this Hamiltonian that the mass for the Dirac electrons is given by the magnetization m_z and the Rashba SOI coupling α (but not the SC order parameter Δ). In this case we have anomalous Hall coefficient for only the + chiral band, and hence find a higher value of the AHC here as compared to case II.

Case IV: $m_z \simeq m_z^*$

The effective low-energy 2×2 Hamiltonian is derived from an expansion of the full 4×4 Hamiltonian around $(k_x, k_y) = (\pm\pi, 0)$ and $(0, \pm\pi)$ and $m_z \simeq m_z^*$. We choose k_x and k_y as small deviations (k) from 0 and π for convenience in the calculation. Here the eigenvalues of the two bands closest to the chemical potential are E_1 and $E_2 = -E_1$ given by

$$\begin{aligned} E_1 &= \\ &\sqrt{m_z^2 + \Delta^2 + \mu^2 + \alpha^2 k^2 - 2\sqrt{(\Delta^2+\mu^2)m_z^2 + \mu^2\alpha^2 k^2)}} \\ &= \sqrt{m_z^2 + m_z^{*2} + \alpha^2 k^2 - \sqrt{m_z^2(m_z^{*2} + 2\mu^2\alpha^2 k^2)}} \ , \end{aligned} \tag{S26}$$

where $m_z^* = \sqrt{\Delta^2+\mu^2}$ and we have taken $\sin k \sim k$ to lowest order. Observe that for $m_z \to m_z^*, k \to 0$, $E_1 = 0 = E_2$, i.e., the band gap vanishes. Thus, the "mass" term of the effective 2×2 Hamiltonian can be written as $(m_z - m_z^*)\sigma_z$ (to lowest order in $m_z - m_z^*$). To obtain the other terms in the effective 2×2 Hamiltonian, we write the energy E_1 as

$$\begin{aligned} E_1 &= \sqrt{m_z^2 + m_z^{*2} + \alpha^2 k^2 - 2m_z m_z^* \sqrt{1 + (\frac{\mu\alpha k}{m_z m_z^*})^2}} \\ &\simeq \sqrt{m_z^2 + m_z^{*2} + \alpha^2 k^2 - 2m_z m_z^* (1 + \frac{\mu^2\alpha^2 k^2}{2m_z^2 m_z^{*2}})} \\ &= (m_z^2 + m_z^{*2} - 2m_z m_z^* + \alpha^2 k^2 (1 - \frac{\mu^2}{m_z m_z^*}))^{1/2} \\ &= (1 - \frac{\mu^2}{m_z^{*2}})^{1/2} \alpha k \quad \text{for} \quad m_z = m_z^* \ . \end{aligned} \tag{S27}$$

This gives the velocity of the Dirac electrons as $v = \alpha(1 - \frac{mu^2}{m_z^{*2}})^{1/2}$. In this way, we find the effective 2×2 Hamiltonian can be written as shown in the main text

$$H_+(\mathbf{k}) = (v \sin k_y)\sigma_x + (v \sin k_x)\sigma_y + (m_z^* - m_z)\sigma_z \ . \tag{S28}$$

D. The topological nature of the ground states, the excitations and the quantum phase transition

We begin this section by discussing briefly the topological nature of the Dirac Hamiltonian, as shown by Volovik[S1]. We consider here a generic Hamiltonian for a system of 2+1D massive Dirac electrons

$$H = v(\sigma_x p_x + \sigma_y p_y + m\sigma_z/v) \ , \tag{S29}$$

where v is the velocity of the Dirac electrons and m their mass. This eigenspectrum has two branches $E = \pm v\sqrt{p_x^2 + p_y^2 + m^2}$. The two branches are separated by the mass m and touch each other at $m = 0$. It is then possible to define a topological Chern invariant for this system[S1]

$$\tilde{N}_3 = \frac{1}{24\pi^2}\epsilon_{\mu\nu\lambda}\mathbf{Tr}\int d^2p dp_0 G\partial_{p_\mu}G^{-1}\, G\partial_{p_\nu}G^{-1}\, G\partial_{p_\lambda}G^{-1} \ , \tag{S30}$$

where $p_0 \equiv E$ (the energy), the Matsubara Greens function is given by

$$G = (ip_0 - H(\vec{p}, m))^{-1} \ , \tag{S31}$$

and the trace **Tr** is taken over all eigenstates of the system. We can see immediately that the G has a singularity at $(p_0 = 0, p_x = 0, p_y = 0, m = 0)$: the Dirac point for the case of the massless Dirac spectrum. For the case of a finite, non-zero mass m, the system is gapped and the Greens function is regular everywhere in 3-momentum space $p_\mu = (p_0, p_x, p_y)$. For the case of $m < 0$ (which corresponds to $m_z < m_z^*$ in the original electronic problem), one finds $\tilde{N}_3 = -1/2$ while for $m > 0$ ((which corresponds to $m_z > m_z^*$), one finds $\tilde{N}_3 = +1/2$. These two cases correspond to the existence of half-hedgehog topological defects in 3-momentum space: for $m < 0$, this is the "anti-meron-hedgehog" and for $m > 0$, the "meron hedgehog" (see Fig.(S1(a)) and Fig.(S1(c)) respectively). These can equivalently be thought of as magnetic monopoles in the 3-momentum space with strength $\Theta = 0, 1$ respectively; the Berry phase accumulated by making a close circuit around the Dirac string attached to this magnetic monopole is given by $\gamma = 0, 2\pi$ respectively.

For the case of the massless Dirac spectrum, i.e., $m = 0$, the topological Chern invariant which describes the singular point at the origin of 3-momentum space corresponds to a winding number of the mapping of the spherical surface S_2 of $(\sigma_x, \sigma_y, \sigma_z)$ around the singular point onto a 2-sphere of a unit vector $\hat{n}$ [S1]

$$N_3 = \frac{1}{8\pi}\epsilon_{ijk}\int_{S_2} \hat{n}\cdot(\frac{\partial\hat{n}}{\partial p_i}\times\frac{\partial\hat{n}}{\partial p_j}) \ . \tag{S32}$$

For the case of massless 2+1D Dirac electrons, one finds $N_3 = 1$, corresponding to a hedgehog topological defect in 3-momentum space (see Fig.(S1(b))). This can equivalently be thought of as a magnetic monopole in the 3-momentum space with strength $\Theta = 1/2$; the Berry phase accumulated by making a close circuit around the Dirac string attached to this magnetic monopole is given by $\gamma = \pi$. Further, the two Chern invariants N_3 and $\tilde{N}_3$ are related to one another as[S1]

$$N_3(m = 0) = \tilde{N}_3(m > 0) - \tilde{N}_3(m < 0) = 1 \ . \tag{S33}$$

It is also important to note that for $m = 0$, the massless 2+1D Dirac Hamiltonian $H = v(\sigma_x p_x + \sigma_y p_y)$ is invariant under a time-reversal transformation $\sigma_\mu \to -\sigma_\mu$, $p_\mu \to -p_\mu$ $(\mu = x, y)$. This corresponds to an emergent

time-reversal symmetry of the massless Dirac electrons observed at $(k_x, k_y) = (\pm\pi, 0)$ and $(0, \pm\pi)$ in our electronic problem, and should not be confused with the fact that the presence of a finite magnetisation m_z means that the fundamental time-reversal symmetry of the system (related to the electron spin) is already broken. However, the emergent time-reversal symmetry (TRS) for the Dirac electron has an interesting consequence: Kramers theorem[S2] states that there must be a partner for such TRS electrons. In our problem, this corresponds to the emergence of pairs of gapless Dirac spectra, i.e., at $(k_x, k_y) = (\pm\pi, 0)$ and at $(k_x, k_y) = (0, \pm\pi)$. Note that for a Hamiltonian H with TRS invariance, there exists an antiunitary operator T which commutes with H, $[H, T] = 0$. Further, for an eigenstate $|\psi_1\rangle$ of H whose energy is E_1, the commutator of H and T guarantees the existence of another eigenstate of H, $|\psi_2\rangle$, with the same energy: this results from $T|\psi_1\rangle = \pm|\psi_2\rangle$[S2]. $|\psi_1\rangle$ and $|\psi_2\rangle$ are then referred to as a Kramers doublet. This has an important consequence for a spin Hall topological insulator state in the form of a pair counter-propagating helical edge states at every boundary of the system[S3,S4]. Further, the existence of two degenerate zero energy states (the Dirac points) in momentum space needs careful consideration, as a study of the electronic scattering processes between them is key towards understanding the phase transition as m_z is tuned through m_z^*. This is carried out below.

From the above discussion, we can see that the topological feature of the ground state of the low-energy effective Dirac Hamiltonian is associated with topological textures in the spinorial structure of the momentum space of this problem. In order to understand the process by which this topological feature can change through a phase transition, as well as the excitations that drive the transition, we need to examine the appearance of the pairs of gapless Dirac spectra at $(k_x, k_y) = (\pm\pi, 0)$ and $(0, \pm\pi)$ in the bandstructure and the scattering processes that may connect them. Given that the momentum difference required for such scattering is large, we may expect that it can only be significant for the case of sufficiently strongly repulsive short ranged interactions between the massless Dirac electrons. For weakly repulsive interactions, we need to establish their relevance for the low-energy physics through renormalisation group (RG) scaling transformations. This gives insight into whether the degeneracy of the two pairs of Dirac nodes can be lifted, and whether gaps can be opened in the Dirac spectra. The problem is further complicated by the fact that these Dirac quasiparticles carry Berry phases, as also seen from the discussion of the topological invariants above.

The answers to these questions is achieved by constructing a non-linear sigma model (NLSM) theory that describes the long-wavelength, low-energy dynamics of the order parameter field describing the scattering of quasiparticles within each of the two pairs of Kramers doublet Dirac cones at $(k_x, k_y) = (\pm\pi, 0)$ and $(0, \pm\pi)$. In this, we are guided by Senthil and Fisher[S5], who following the classic work of Abanov and Wiegmann[S6], showed that the $N = 2$ QED_3 theory in 2+1D is equivalent to the O(4) NLSM in 2+1D with a topological Θ-term and a value of the topological angle $2\pi\Theta = \pi$. For the sake of completeness, we sketch briefly their approach and results here, before proceeding to study the phase transition through an alternate approach involving the non-trivial edge states of the system. We start by identifying the low-energy theory of a given Kramers doublet pair of Bogoliubov-de Gennes (BdG) quasiparticles with Dirac dispersion as a $N = 2$ QED_3 theory in Euclidean 3D, consisting of 2 "flavours" of two-component Dirac fermions ψ coupled to a non-compact $U(1)$ gauge field A:

$$S = \int d^3x \bar{\psi}(\tau_i(-i\partial_i - A_i))\psi + \frac{1}{2e^2}(\epsilon_{ijk}\partial_j A_k)^2 \ , \quad \text{(S34)}$$

where the τ_i are the Pauli matrices. A similar theory can be constructed for the other Kramers doublet pair as well. This action has a global $SU(2) \times SU(2)$ symmetry, where each of the two $SU(2)$ reflects on an invariance associated with unitary rotations that transform one of the two Dirac fermion flavours of a given Kramers doublet into the other. We then focus on scattering processes involving both flavours of Dirac electrons within each Kramers doublet. Such processes describe the separate ordering tendencies of the two $SU(2)$ vectors, each of which can be written as $\bar{\psi}\sigma\psi$ (where σ characterises the 2-component "flavour" space). For a given Kramers doublet, this can be introduced via a short-ranged repulsive inter-flavour interaction term

$$S_{\text{int}} = \int d^3x \Lambda(\bar{\psi}\sigma\psi)^2 \quad , \quad \Lambda > 0 \ . \quad \text{(S35)}$$

Now, employing a Hubbard-Stratonovich transformation, we can decouple this four-fermion interaction in terms of a $O(3)$-symmetric order parameter vector field $\vec{N}$ whose magnitude is the mass ($m_e > 0$) that can be generated for the Dirac quasiparticles by the 2-particle scattering processes (shown in Fig.(S2(a))), $\vec{N} = m_e \ \vec{n} = m_e \ (\phi_1, \phi_2, \phi_3)$, $\vec{n}^2 = 1$:

$$\frac{m_e^2 \vec{n}^2}{2\Lambda} + i \ m_e \vec{n} \cdot \bar{\psi}\vec{\sigma}\psi \ . \quad \text{(S36)}$$

Note that the first term is a constant with no dynamics as $\vec{n}^2 = 1$. Thus, we write the total action as:

$$S = \int d^3x \bar{\psi}(\tau_i(-i\partial_i - A_i) + i \ m_e \vec{n}\cdot\vec{\sigma})\psi + \frac{1}{2e^2}(\epsilon_{ijk}\partial_j A_k)^2 \ . \quad \text{(S37)}$$

By following the technique developed by Abanov and Wiegmann[S6], one can integrate out the fermion fields by computing the fermionic determinant and carrying out an expansion in $1/m_e$, as well as integrate out the gauge field A. Senthil and Fisher[S5] show that the resulting theory is the O(4) NLSM in 2+1D, but with a Θ-term which describes the topological defects of this theory. This NLSM is written in terms of a field U which

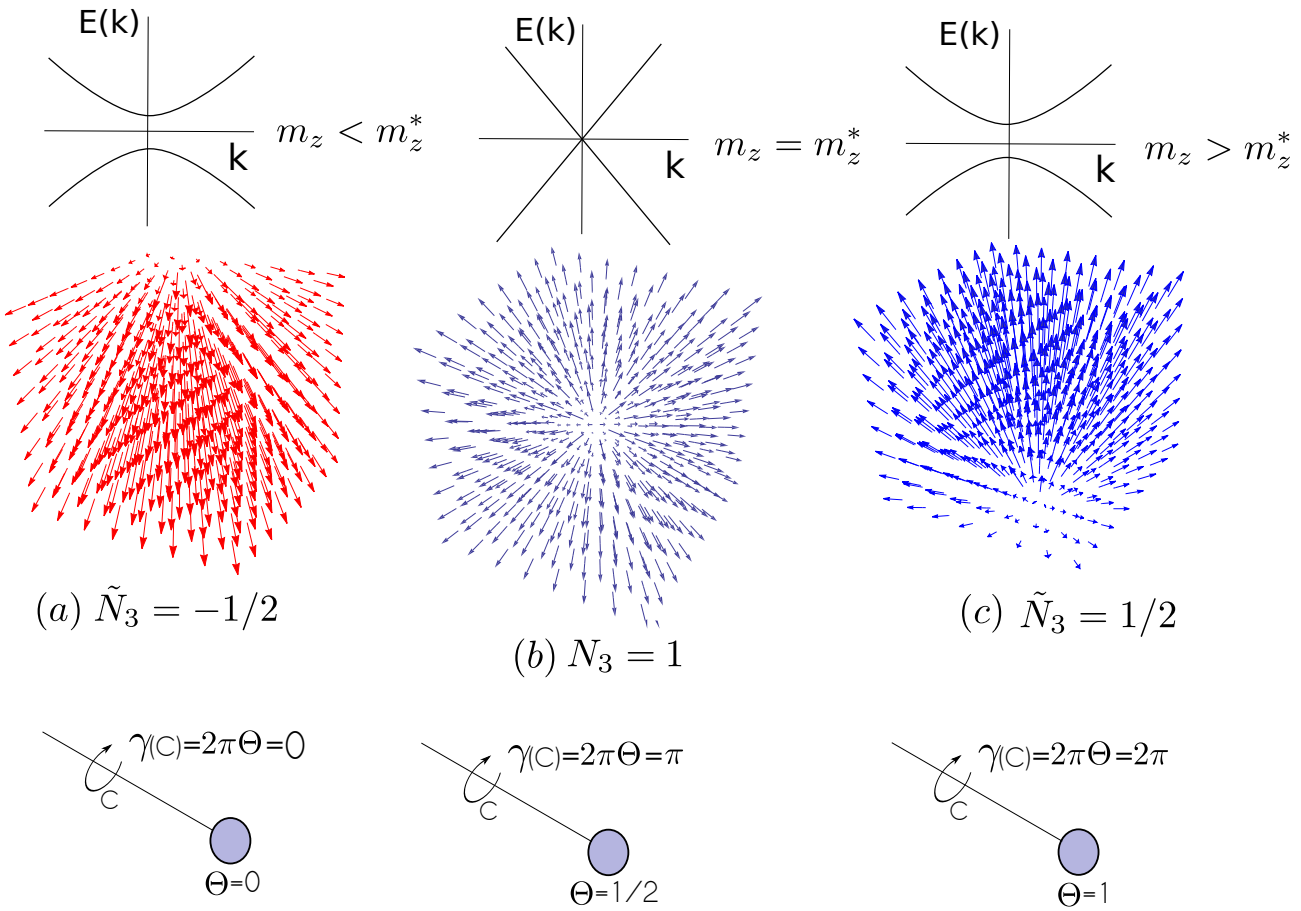

FIG. S1. (Color online) The topological Chern invariant associated with the momentum space structure of the massive Dirac equation as m_z is tuned through m_z^*. (a) For $m_z < m_z^*$, the massive Dirac spectrum possesses a Chern invariant $\tilde{N}_3 = -1/2$ corresponding to a half-hedgehog (or "meron hedgehog") in momentum space. This topological defect is equivalent to a magnetic monopole of strength $\Theta = 0$, with a Dirac string around which a Berry phase $\gamma = 2\pi\Theta = 0$ is accumulated in the circuit C. (b) For $m_z = m_z^*$, the massless Dirac spectrum has a Chern invariant $N_3 = \tilde{N}_3(m_z > m_z^*) - \tilde{N}_3(m_z < m_z^*) = 1$ corresponding to a hedgehog in momentum space. This topological defect is equivalent to a magnetic monopole of strength $\Theta = 1/2$, with a Dirac string around which a Berry phase $\gamma = \pi$ is accumulated in the circuit C. (c) For $m_z > m_z^*$, the massive Dirac spectrum possesses a Chern invariant $\tilde{N}_3 = -1/2$ corresponding to an anti-half-hedgehog (or "anti-meron hedgehog") in momentum space. This topological defect is equivalent to a magnetic monopole of strength $\Theta = 1$, with a Dirac string around which a Berry phase $\gamma = 2\pi$ is accumulated in the circuit C.

depends on a 4-component unit vector (all of whose elements are real) $\vec{\phi} = (\phi_0, \phi_1, \phi_2, \phi_3)$ on the three dimensional spherical surface (S^3). U is an element of the compact SU(2) Lie group. The fact that this Lie group has a nontrivial homotopy group $\pi_3[\mathrm{SU}(2)] = Z$ (corresponding to the integer number of coverings of space-time coordinate space by the $\vec{\phi}$ field configuration) signals the presence of topological defect excitations of this NLSM theory. The charge of these topological defects reflects on the Chern invariant/Berry phase $\tilde{N}_3$ of the 2+1D Dirac electrons discussed earlier. The component ϕ_0 characterises valence bond (VBS/dimer) order in the system and relates to the Umklapp backscattering process of a pair of electrons between the two Dirac cones. This is shown in Fig.(S2(b)). Importantly, ϕ_0 also characterises the half-hedgehog (or "meron-hedgehog"[S5]) topological defects: the sign of ϕ_0 relates to the two values of $\tilde{N}_3 = \pm 1/2$. Further, the dynamics of ϕ_0 opens the door towards changes in this topologically invariant quantity through the generation of hedgehog instanton excitations (with topological charge $N_3 = 1$).

The O(4) NLSM theory in 2+1D[S5,S7] written in terms of the 4-component field $\vec{\phi}$ can be written as $S = S_0 + i2\pi\Theta Q$, where

$$S_0 = \int d^2x d\tau \frac{1}{g}(\partial_\mu \vec{\phi})^2 \ , \tag{S38}$$

and the topological charge Q of the meron-hedgehogs is given by

$$Q = \frac{1}{12\pi^2}\int d^2x d\tau \epsilon_{\mu\nu\rho}\epsilon_{abcd}\phi^a \partial_\mu \phi^b \partial_\nu \phi^c \partial_\rho \phi^d \ . \tag{S39}$$

The topological Chern invariant $\tilde{N}_3$ obtained earlier from the low-energy effective Dirac Hamiltonian is, in fact,

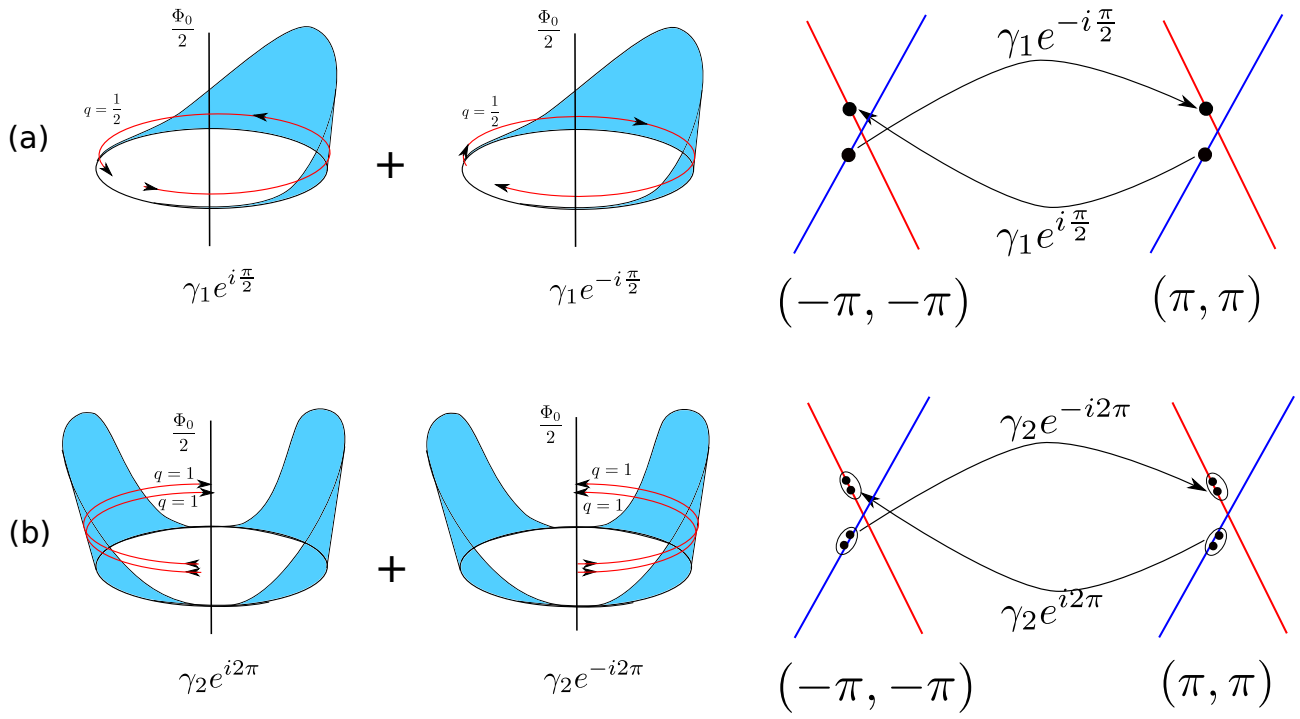

FIG. S2. (Color online) Single-particle backscattering and 2-particle Umklapp scattering between the two Dirac cones and their corresponding instanton tunneling processes. In (a), we show that the single particle backscattering is equivalent to an instanton event in which a particle with (topological) charge $q = 1/2$, confined on a circle (characterised by an angle ϕ) with a $\cos\phi$ potential, tunnels from $\phi = 0$ to $\phi = 2\pi$ (and vice versa) with tunnel amplitude γ_1. The circle is threaded by an Aharanov-Bohm (AB) flux $\Phi_0/2$, such that the instanton and anti-instanton pick up AB phases of $e^{i\pi/2}$ and $e^{-i\pi/2}$ respectively during the tunneling event. In (b), we show that the Umklapp scattering process is equivalent to an instanton event in which 2 particles, each with (topological) charge $q = 1$, confined on a circle (characterised by an angle ϕ) with a $\cos 2\phi$ potential tunnels from $\phi = 0$ to $\phi = \pi$ (and vice versa) with tunnel amplitude γ_2. The circle is threaded by an Aharanov-Bohm (AB) flux $\Phi_0/2$, such that the instanton and anti-instanton pick up AB phases of $e^{i2\pi}$ and $e^{-i2\pi}$ respectively during the tunneling event.

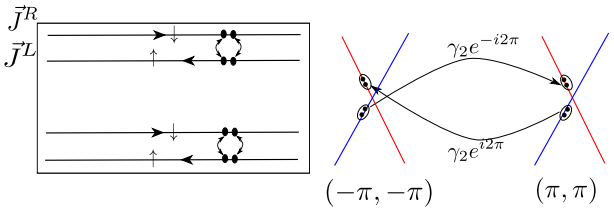

FIG. S3. (Color online) Umklapp scattering of 2 electrons between the 2 oppositely directed helical edges of the spin Hall phase in our system.

equivalent to the topological charge Q of the meron-hedgehog defect configurations in the NLSM theory. The topological angle $2\pi\Theta = \pi$ for the case of massless Dirac electrons in the original electronic problem (i.e., $m_z = m_z^*$), while a finite mass for the Dirac electrons achieved for $m_z < m_z^*$ and $m_z > m_z^*$ corresponds to $2\pi\Theta < \pi$ and $2\pi\Theta > \pi$ respectively. In this way, the system undergoes a Lifshitz transition in which the topology of the electronic momentum space is changed as m_z is tuned through m_z^*[S1,S8]. At $2\pi\Theta = \pi$, the $T = 0$ path integral of the system enjoys a discrete symmetry under a parity transformation of the four-vector $\vec{\phi} \to -\vec{\phi}$; this corresponds to an invariance under (Euclidean) time reversal transformation $i\tau \to -i\tau$ together with a parity transformation $(x, y, z) \to (-x, -y, -z)$. At this value of Θ, one can equally as well see this as an invariance of the system under the parity transformation $\Theta \to -\Theta$; this is also true of the trivial values of $2\pi\Theta = 0, 2\pi$. This discrete symmetry protects the topological angle from changing under RG transformation at these three values of $2\pi\Theta = 0, \pi, 2\pi$, while its flow under RG for all other values is not forbidden. At this point, we note that the appearance of the topological Θ-term in the action give rise to the possibility of quantum interference in the free-energy landscape from which the quantum partition function is constructed. This arises from the complex-valued phase factors associated with different configurations of the system. It also shows that the true quantum many-body ground state is achieved via non-perturbative instanton tunneling events between various perturbative ground states which possess fixed values of the topological charge Q and are weighted by Θ-dependent phase factors. Such linear-superposition quantum ground states are called Θ-vacua, and give rise to an oscillatory dependence of the energy separation between the ground state and the lowest lying excited state on the topological angle Θ[S9].

The production and proliferation of such instantons,

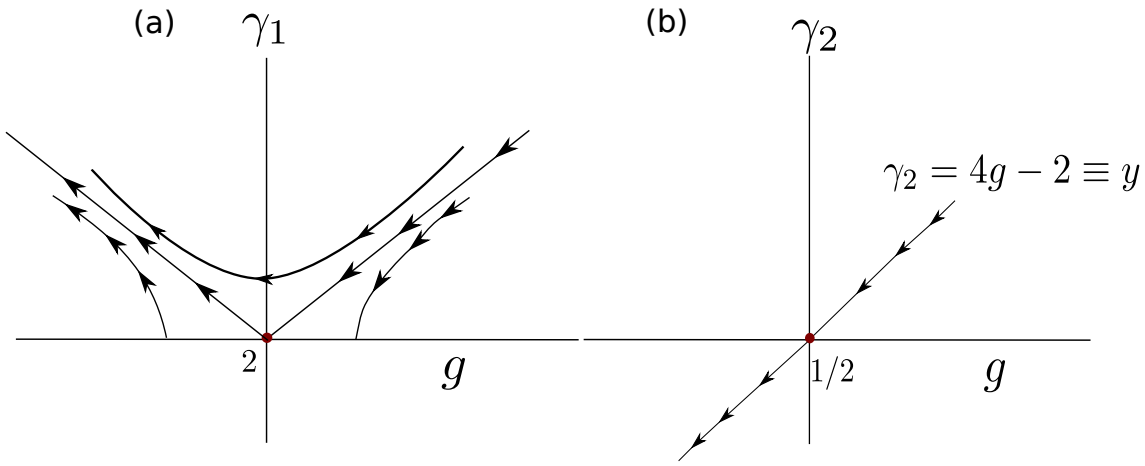

FIG. S4. (Color online) The RG phase diagrams for the Berezinskii-Kosterlitz-Thouless (BKT) and Wess-Zumino-Novikov-Witten (WZNW) phase transitions. The diagram (a) is the BKT RG phase diagram displayed in terms of the NLSM coupling g versus the single instanton tunnel amplitude γ_1. The separatrices $|g| = \gamma_1$ separate the RG trajectories leading towards the line of weak coupling fixed points $\gamma_1 = 0$, $g \geq 2$ from those leading towards the strong coupling fixed point in γ_1. The diagram (b) is the WZNW RG phase diagram displayed in terms of the NLSM coupling g versus the doubled instanton tunnel amplitude γ_2. The RG flow on the $SU(2)$ symmetric line $\gamma_2 = 4g - 2$ indicates the WZNW phase transition, with γ_2 being a dangerously irrelevant coupling under the RG transformations: for $\gamma_2 > 0$, the RG flow leads towards the $SU(2)$ symmetric weak-coupling fixed point theory at $g = 1/2$, $\gamma_2 = 0$ (with a unique ground state) while for $\gamma_2 < 0$, the RG flow leads towards the strong coupling fixed point theory (with a doubly-degenerate ground state).

therefore, needs careful consideration. For instance, the topological defect instanton excitations that can change the value of a given Q are expected to be suppressed by a large mass for the Dirac electrons. Should this be the case, we may expect to reach conclusions from studying only the kinetic part of the NLSM action. This is achieved by breaking the O(4) symmetry of the NLSM given above down to $\mathrm{O}(3) \times Z_2$, and studying the effective dynamics of the remnant O(3) NLSM theory in 2+1D. Senthil and Fisher[S5] argued, however, that our expectations could be belied for a special value of the topological angle $2\pi\Theta = \pi$. Here, the ordered phase of the O(3) theory with a unique ground state can be rendered critical due to Berry phase-carrying meron-hedgehog and hedgehog instanton tunneling events (see Fig.(S1)) that interpolate between the ordered ground state and an excited state that lies vanishingly close. Remarkably, the single meron-hedgehog instanton excitation is unable to lead to the formation of a gap between the ground state and the lowest excited state due to a destructive interference mechanism arising from the Aharanov-Bohm (AB) like Berry phases (given by the topological angle $2\pi\Theta = 2\pi(\Phi_{\mathrm{AB}}/\Phi_0) = \pi$) accumulated along the multiply connected field-configuration manifold that connects these two states. A similar gaplessness of the 1+1D $O(3)$ NLSM at $\Theta = \pi$ was also noted earlier[S10]. However, the doubled hedgehog instantons undergo a constructive interference by the same token. If the tunneling of such doubled hedgehog instantons is RG irrelevant, the ordered O(3) NLSM theory at $2\pi\Theta = \pi$ corresponds to the emergent spin Hall theory in the original electronic problem. This is shown in Fig.(S2).

On the other hand, if these doubled instantons are RG relevant, they may destabilise the ground state even in the absence of any explicit symmetry-breaking perturbations. The RG flow then leads away from the critical theory, opening a gap above a doubly degenerate ground state of the infra-red (IR) strong coupling fixed point theory. In this case, Senthil and Fisher propose that the emergent state has no order in the O(3) order parameter but possesses Z_2 topological order. For an O(3) order parameter which characterises Neél ordering of S= 1/2 spins in a 2D rectangular lattice, this topological state is a Z_2 spin liquid[S5]. In this way, we expect that the emergent spin Hall phase observed at criticality in our electronic problem can have an instability leading to a state with Z_2 topological order and a doubly degenerate ground state. Further, this state is expected to have fractionalised excitations that make the transitions between the two topologically degenerate ground states. Applying explicit symmetry-breaking terms to this O(3) NLSM theory (e.g., through a uniform external B-field) will shift the value of the topological angle away from $2\pi\Theta = \pi$. The single instanton excitation will then no longer vanish from the interference mechanism. Instead, given that these single instantons are typically RG relevant, they will gap the Dirac-spectrum of the electronic problem, leading to the two gapped anomalous Hall effect (AHE) theories on either side of the phase transition.

As we will now show, this transition can also be captured by developing a theory for the boundary or edge states of this system. The quasiparticle band diagram reveals that the phase transition involves a ground state level crossing without the bulk gap vanishing everywhere. This is an example of a first order phase transition. The presence of the bulk gap allows us to focus on a way

to view the passage through the band-crossing in the bulk via a theory of the massless 1D Dirac electrons at edge[S7]; this is the essence of the bulk-boundary correspondence[S11]. Thus, we seek the edge theory for when the bulk is at criticality, i.e., the case of the anisotropic 2+1D O(4) NLSM with O(3) order at a value of the topological angle $2\pi\Theta = \pi$. Here, we are guided by the fact that the topological term Q of the O(4) NLSM theory in 2+1D given above with $2\pi\Theta = \pi$ is identical to the Wess-Zumino-Novikov-Witten (WZNW) term of the 1+1D Tomonaga Luttinger liquid for spinless fermions or the Heisenberg spin-1/2 chain with nearest neighbour antiferromagnetic exchange interactions[S5]:

$$\Gamma[U] = \frac{i}{12\pi}\epsilon_{\mu\nu\rho}\mathrm{tr}[(U^\dagger\partial_\mu U)(U^\dagger\partial_\nu U)(U^\dagger\partial_\rho U)] \ , \quad \text{(S40)}$$

where the field U is an element of the $SU(2)$ group once again, and defines a map from S^2 to S^3. The topological WZNW term Γ is defined in by the area traced out by the field U which encloses the volume S^3. The field U describes a "superspin" which combines the valence bond solid (VBS) order parameter (ϕ_0) and the three component Neél order parameter $\vec{\phi} = (\phi_1, \phi_2, \phi_3)$:

$$U = \phi_0 + i\phi_1\sigma_x + i\phi_2\sigma_y + i\phi_3\sigma_z \ \ , \ \ \phi_0^2 + \vec{\phi}^2 = 1 \ . \quad \text{(S41)}$$

Then, following the classic works of Witten[S12], as well as Knizhnik and Zamolodchikov[S13], we may identify the edge state theory at the critical point as the $SU(2)_{k=1}$ (i.e., the level-1) WZNW theory of the Heisenberg spin-1/2 chain with nearest neighbour antiferromagnetic interactions. As guaranteed by the Lieb-Schultz-Mattis (LSM) theorem[S14], this system has a unique ground state at the SU(2) symmetric Heisenberg critical point corresponding to the 1D algebraic spin liquid[S5]. The action for the $SU(2)_k$ (i.e., the level-k) WZNW theory is given by

$$S = \int d\tau dx \frac{1}{2g}\mathrm{tr}[\partial_\mu U^\dagger \partial_\mu U] + k\Gamma[U] \ . \quad \text{(S42)}$$

Witten showed that the topological coupling k affects the RG flow of the NLSM coupling g in this WZNW theory[S12]

$$\frac{dg}{dl} = [1 - (\frac{k\ g}{4\pi})^2]\ (\frac{g}{4\pi}) \ . \quad \text{(S43)}$$

This RG equation shows the existence of a non-trivial stable fixed point at $g^* = 4\pi/k$. Put together with the fact that at this value of g^*, the theory can be written using the non-Abelian bosonisation formalism in terms of free bosons which satisfy a $SU(2)_k$ Kac-Moody current algebra, Witten conjectured that the WZNW theory must have an exact fixed point at g^*. Using conformal field theoretic methods, this was shown to be correct by Knizhnik and Zamolodchikov[S13]. In this way, we identify the $SU(2)_{k=1}$ WZNW theory with NLSM coupling $g^* = 4\pi$ (corresponding to the topological angle $2\pi\Theta = \pi$) as the spin Hall critical theory (with two oppositely directed 1D helical edge modes corresponding to massless 1D Dirac electrons of both helicities) at the phase transition between the two AHE ordered ground states (i.e., with a gapped bulk and only one chiral 1D edge mode of massless Dirac electrons) of our original electronic problem.

But under what conditions is this critical theory stable, and what are its instabilities? As shown in Ref.[S11], the $SU(2)_{k=1}$ WZNW theory is stable against perturbations involving the backscattering coupling between chiral spin currents, $g_1\ \vec{J}_R \cdot \vec{J}_L$. Here, $\vec{J}_{R/L}$ correspond to the right- and left-moving chiral spin currents respectively of the 1+1 edge theory: $J_R^a(x) = \frac{1}{2}\psi^\dagger_{R,\sigma}(x)\tau^a_{\sigma,\sigma'}\psi_{R,\sigma'}(x)$, $J_L^a(x) = \frac{1}{2}\psi^\dagger_{L,\sigma}(x)\tau^a_{\sigma,\sigma'}\psi_{L,\sigma'}(x)$, where $a = (1,2,3)$ and τ^a are the three Pauli matrices. The coupling g_1 corresponds to the amplitude of spin-flip backscattering of electrons between the two oppositely directed 1D helical edge states on a given edge of the spin Hall system arising from electronic correlations. The RG equation for g_1 is

$$\frac{dg_1}{dl} = -\frac{2}{\pi}g_1^2 \ . \quad \text{(S44)}$$

Thus, we can see that the case of a symmetry-preserving perturbation corresponds to the coupling $g_1 > 0$: here, g_1 is marginally irrelevant and can neither break the $SU(2)$ symmetry dynamically, nor open a gap in the spectrum. This corresponds to the case of the emergent time-reversal symmetry (TRS) associated with the gapless Dirac spectra at the spin Hall critical point being robust against perturbations that may break it spontaneously. Conversely, for the case of $g_1 < 0$, the $SU(2)$ symmetry of the WZNW theory (i.e., the TRS of the underlying Dirac theory) is spontaneously broken: g_1 is now marginally relevant, flows to strong coupling and opens a gap in the spectrum above a doubly-degenerate ground state characterised by the spontaneous dimerisation of the spins (i.e., valence bond order). This change in RG behaviour with the change in the sign of g_1 is known as the WZNW-type transition[S15], and needs the inclusion of a competing next nearest neighbour antiferromagnetic exchange coupling between the spins which exceeds a critical value (see Ref.([S16]) and references therein). In the original electronic problem, this would correspond to the possibility of gapping the Dirac electrons at the edge (i.e., localising them) via scattering from repulsive interactions with extended range, as shown in Fig.(S3). This can happen through Umklapp (i.e., 2-particle) backscattering effects between the 2 helical edge states. Localisation via Umklapp scattering mediated by quenched disorder at the edge can also destabilise this theory and localise the electrons at the edge[S17,S18]. In this way, we see that the transitions seen from theories of the bulk as well as that for the edge lead to doubly degenerate ground states with Z_2 topological order. Interestingly, however, the critical theory in the bulk possesses O(3) order in the ground state while that at the edge is the

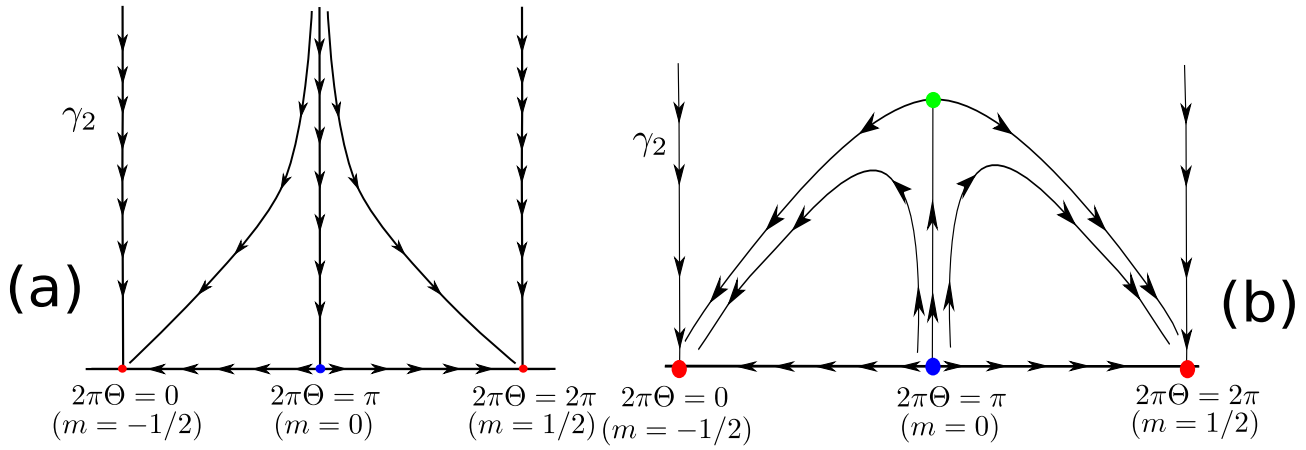

FIG. S5. (Color online) The RG phase diagrams obtained from the scaling equations for γ_2 and m. Recall that the topological angle $\Theta = S - m$, and its scaling can be equivalently seen to track that of the single instanton tunnel amplitude γ_1 (see main text for discussion). (a) The RG phase diagram for the case of $\gamma_2 > 0$ being marginally irrelevant. The RG flow for $2\pi\Theta = \pi$ leads towards the stable weak coupling fixed point theory (blue dot) which corresponds to the emergent spin Hall phase in our problem. All RG flows for $2\pi\Theta \neq \pi$ involve an explicit breaking of the emergent $SU(2)$ symmetry at $2\pi\Theta = \pi$ via the scaling of the single instanton tunnel amplitude γ_1, and lead to the AHE fixed point theories (red dots) with gapped ground states at $2\pi\Theta = 0, 2\pi$ $(m = -1/2, 1/2)$. Note the symmetry $m \to -m$ of the RG phase diagram about $m = 0$. γ_2 is RG irrelevant at $2\pi\Theta = 0, 2\pi$. (b) The RG phase diagram for the case of $\gamma_2 < 0$ being marginally irrelevant. The RG flow for $2\pi\Theta = \pi$ leads towards the strong coupling fixed point theory (green dot) which corresponds to the Z_2 topological insulator with a doubly degenerate ground state. All other RG flows are as in case (a). The dangerous irrelevance of γ_2 and its appearance in the theory only at $2\pi\Theta = \pi$ makes the phase transition at this value of the topological angle a case of deconfined quantum criticality.

fluctuation disordered algebraic spin-liquid state of the $SU(2)_1$ WZNW theory. This difference is guaranteed by the Mermin-Wagner-Hohenberg theorem[S19] which forbids ordering at any finite temperature in 2D systems, in conjunction with the Lieb-Schultz-Mattis (LSM)[S14] theorem for the 1+1D Heisenberg spin-1/2 chain with nearest neighbour antiferromagnetic exchange interactions.

We can now address the perturbations that appear upon breaking the global $SU(2)$ symmetry of the action, i.e., by departing from the special value of the topological angle $2\pi\Theta = \pi$. This will help in displaying the fact that there exists an analog of the subtle interference mechanism discussed earlier for instantons of the 2+1D O(3) NLSM which also renders the 1+1D WZNW theory with $2\pi\Theta = \pi$ stable. Following Affleck[S20], it is convenient to consider the role played by topological excitations through the sine-Gordon version of the 1+1D O(3) NLSM Lagrangian:

$$L = \frac{1}{2}(\partial_\mu \phi)^2 + \sum_{n,q_n} \gamma_n \exp^{i(n\sqrt{g}\phi + 2\pi n q_n \Theta)} - \frac{m}{\pi}\partial_x \phi \ . \tag{S45}$$

Here, ϕ is the scalar field encoding the Neèl order, g is the phase stiffness parameter/NLSM coupling, n is the vorticity of the topological excitations in the field ϕ, q_n is the charge of the topological excitation and γ_n the fugacity for an instanton excitation with vorticity n, and the topological angle is $\Theta = S - m$[S21]. Note that S is the spin quantum number of the constituent spins in the problem and m is the magnetisation; $S = 1/2$ corresponds to the case of gapless Dirac electrons and $m \equiv m_z - m_z^*$ in the original electronic problem. The first term gives the cost of generating collective excitations, the second and third the cost of topological excitations and the fourth the effect of an explicit symmetry-breaking B-field (through the magnetisation m). The bare value of the instanton fugacity can be computed using standard instanton techniques[S9], and $\gamma_1 \sim \exp(-S_0/\hbar)$, where S_0 is the classical Euclidean action for the instanton of the sine-Gordon problem. As shown by Affleck[S20], this simplest instanton excitation has $n = \pm 1$ and each value of n has two charges $q_n = \pm 1/2$ (which corresponds to the two values of the Chern no. $\tilde{N}_3$ discussed earlier for the electronic problem). In the absence of an external B-field, $m = 0$, and with $S = 1/2$, we have $\Theta = 1/2$. Then, in this case, we have

$$\begin{aligned} &\sum_{n=\pm 1, q_n = \pm 1/2} \gamma_1 \exp^{i(n\sqrt{g}\phi + 2\pi n q_n \Theta)} \\ &= \gamma_1 (\exp^{i\pi/2} + \exp^{-i\pi/2})(\exp^{i\sqrt{g}\phi} + \exp^{-i\sqrt{g}\phi}) \\ &= 4\gamma_1 \cos(\pi/2)\cos(\sqrt{g}\phi) \ = \ 0 \ . \end{aligned} \tag{S46}$$

In this way, we can see that while these instanton excitations are RG relevant (the coupling γ_1 has a scaling dimension $g < 1/2$), it is suppressed via a destructive interference mechanism for $2\pi\Theta = \pi$ and thus unable to open a gap in the spectrum[S20] (consult Fig.(S2)(a)). However, the instantons with doubled vorticity $n = \pm 2$ with topological charges $q = \pm 1$ are hedgehog excitations (where $|q| = 1$ corresponds to the value of the Chern no. N_3 discussed earlier for the case of massless Dirac electrons) which undergo a constructive interference even at

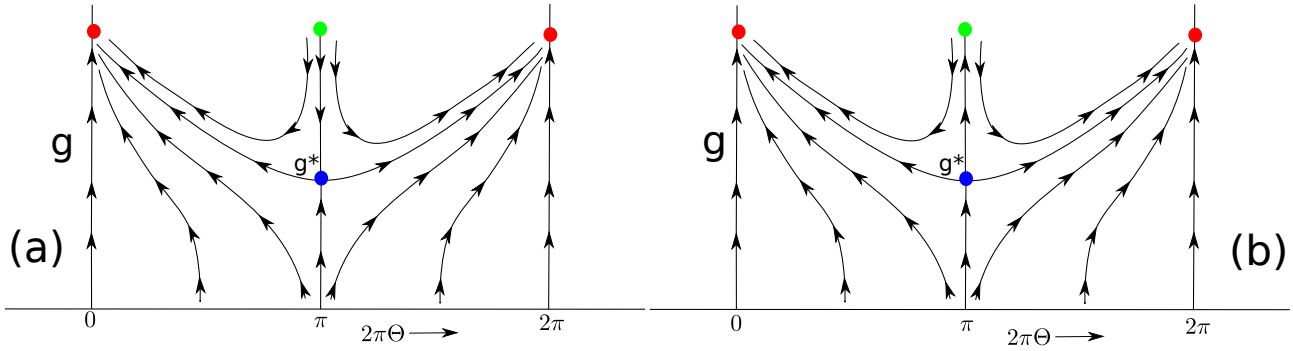

FIG. S6. (Color online) The RG phase diagrams obtained from the scaling equations for the NLSM coupling g and the topological angle Θ. (a) The RG phase diagram for the case of the doubled instanton tunnel coupling $\gamma_2 > 0$ being marginally irrelevant. The RG flows for $2\pi\Theta = \pi$ leads towards the intermediate coupling fixed point theory at $g = g^* = 4\pi$ (blue dot) which corresponds to the emergent spin Hall phase in our problem. All RG flows for $2\pi\Theta \neq \pi$ lead to the AHE fixed point theories (red dots) with gapped ground states at $2\pi\Theta = 0, 2\pi$. Note the symmetry of the RG phase diagram $\Theta \to -\Theta$ about $\Theta = 1/2$. g is RG relevant at $2\pi\Theta = 0, 2\pi$. (b) The RG phase diagram for the case of $\gamma_2 < 0$ being marginally irrelevant. The RG flow for $2\pi\Theta = \pi$ now leads away from the intermediate fixed point at g^* towards the strong coupling fixed point theory (green dot) which corresponds to the Z_2 topological insulator with a doubly degenerate ground state. All other RG flows are as in case (a). The change in the nature of the RG flow about g^* for $2\pi\Theta = \pi$ brought about by the dangerous irrelevance of γ_2 makes the phase transition at this value of the topological angle a case of deconfined quantum criticality.

$2\pi\Theta = \pi$ by the same token (consult Fig.(S2)(b))

$$\begin{aligned}&\sum_{n=\pm 2, q_n=\pm 1} \gamma_2 \exp^{i(n\sqrt{g}\phi + 2\pi n q_n \Theta)} \\ &= 4\gamma_2 (\exp^{i2\pi} + \exp^{-i2\pi})(\exp^{i2\sqrt{g}\phi} + \exp^{-i2\sqrt{g}\phi}) \\ &= 4\gamma_2 \cos(2\pi)\cos(2\sqrt{g}\phi) \;=\; 4\gamma_2 \cos(2\sqrt{g}\phi)\ . \end{aligned} \tag{S47}$$

The RG equations for g and γ_2 are given by

$$\frac{dg}{dl} = -\frac{\gamma_2^2}{4} \quad , \quad \frac{d\gamma_2}{dl} = (2 - 4g)\gamma_2\ . \tag{S48}$$

As discussed earlier, there is no RG equation for the Θ parameter for the case of $m = 0$ due to the existence of an extra discrete symmetry of the theory. While the two RG equations given above describe the Berezinskii-Kosterlitz-Thouless (BKT)[S22] universality class of transitions, it also describes the WZNW universality class. This can be seen as follows[S15]: first denote $y_0 = 4g - 2$, $y_1 = \gamma_2$, then impose the global $SU(2)$ symmetry of the WZNW theory on the sine-Gordon problem by requiring that $y_0 = y_1 \equiv y$ even under the RG transformations. This then gives the RG equation for the lone coupling in the problem as $dy/dl = -y^2$, which is precisely the RG observed for the coupling g_1 of the WZNW theory seen earlier with the redefinition: $g_1 = (\pi/2)y$. From our earlier discussion for g_1, we can see that the coupling y is either marginally irrelevant or marginally relevant, depending on its sign. Further, the $SU(2)$ symmetry of the WZNW fixed point fixes the value of the coupling g of the sine-Gordon theory as $g^* = 1/2$[S16]: this is where the coupling γ_2 is exactly marginal. The RG phase diagrams for the BKT and WZNW transitions is shown in Fig.(S4).

From the identification of the topological angle $\Theta = S - m$[S21], we can also perform a similar RG analysis of the sine-Gordon model for $m \neq 0$. First, we can see immediately that the destructive interference mechanism no longer suppresses the instanton tunnel coupling γ_1 for $m \neq 0$:

$$\begin{aligned}&\sum_{n=\pm 1, q_n=\pm 1/2} \gamma_1 \exp^{i(n\sqrt{g}\phi + 2\pi n q_n \Theta)} \\ &= \gamma_1 (\exp^{i\pi(1/2-m)} + \exp^{-i\pi(1/2-m)})(\exp^{i\sqrt{g}\phi} + \exp^{-i\sqrt{g}\phi}) \\ &= 4\gamma_1 \cos(\pi(1/2 - m))\cos(\sqrt{g}\phi)\ . \end{aligned} \tag{S49}$$

The RG equation for g, γ_1 and the magnetisation m is given as[S16,S23]

$$\begin{aligned}\frac{dg}{dl} &= -\gamma_1^2 J_0(m\alpha) \quad , \quad \frac{d\gamma_1}{dl} = (2 - g)\gamma_1 \\ \frac{dm}{dl} &= m - \frac{\gamma_1^2}{2\pi\alpha} J_1(m\alpha)\ , \end{aligned} \tag{S50}$$

where J_0 and J_1 are Bessel functions that arise from the use of sharp cut-off functions while implementing the RG transformations[S16]. Importantly, the RG equation for m is symmetric under the interchange of $m \to -m$. These RG equations show that the presence of a non-zero m leads to two gapped ground states in which the $SU(2)$ symmetry is explicitly broken and the magnetisation is saturated at $m = -1/2$ and $m = 1/2$ respectively. A large magnetisation will, in turn, lead to a suppression the instanton tunnel amplitude γ_1. This is easily seen in the original electronic problem, where a growing magnetisation m of the spin problem corresponds to the presence of only those massless Dirac electrons at the edge whose spins are aligned with the direction of m_z. Backscattering of these electrons (with an amplitude corresponding to γ_1) is strongly suppressed due to the conservation of their helicity, and is common to other cases in which spin rotation symmetry is explicitly broken by a strong

external magnetic field: the chiral massless Dirac electrons observed at the edge of the quantum Hall effect[S24] and electrons in 1D Tomonaga-Luttinger liquid quantum wire with a large Zeeman gap[S25]. The RG phase diagram for the doubled instanton tunnel amplitude γ_2 versus the topological angle Θ is shown in Fig.(S5).

Note that the values of $m = -1/2, 1/2$ correspond to values of the topological angle $\Theta = 0, 1$. That the theories at $\Theta = 0, 1$ possess gapped spectra is corroborated by the works of Polyakov[S26] and Haldane[S27], who showed that the 1+1D O(3) NLSM theory with a value of the topological angle $2\pi\Theta = 0,\ 2\pi$ has the NLSM coupling g flow to strong coupling under RG. It is then straightforward to identify these two strong coupling fixed points at $\Theta = 0, 1$ as the two AHE theories (with bulk gaps, and a single edge mode of chiral massless Dirac electrons) on either side of the phase transition in our original electronic problem, $m_z << m_z^*$ and $m_z >> m_z^*$. In this way, we are able to see the manner in which instanton excitations drive the Lifshitz transition, changing the topology of the electronic momentum space.

Finally, similar considerations can also be made for the effects of a staggered magnetic field on the system: as discussed by Affleck[S28], such a field couples to the staggered magnetisation m_N and will again change the Θ topological angle, breaking the global $SU(2)$ symmetry and involve a doubling of the unit cell via the establishment of Neél order. Further, it can be shown[S29] that in the presence of explicit dimerisation (i.e. dimer order) in the system, the doubled instanton tunnel amplitude γ_2 will affect the RG equation for the staggered magnetisation m_N in a way analogous to that shown above for the way in which γ_1 affects the RG of the uniform magnetisation m. We show the RG phase diagram for the NLSM coupling g versus the topological angle Θ in Fig.(S6). Importantly, via the bulk-boundary correspondence that is well established for topological insulators[S11], our findings from the edge field theories give evidence for the fact that the dangerous irrelevance of the doubled instanton tunnel amplitude γ_2 observed only at $2\pi\Theta = \pi$, and the subsequent stabilisation of the spin Hall phase in the bulk, is a case of deconfined quantum criticality[S5,S11]. The spin Hall theory for $\gamma_2 = 0$ is a critical fixed point, with three possible unstable directions in terms of the NLSM coupling g, the topological angle Θ and the fugacity for the doubled instantons γ_2. We can, therefore, classify the spin Hall phase as tricritical[S30], with the transition being first order (i.e., involving explicit symmetry breaking) in Θ and continuous in g as well as γ_2.

E. Self-consistent BdG formalism in momentum space

Hamiltonian (1) in the main text is diagonalized via a spin-generalized Bogoliubov-Valatin transformation $\hat{c}_{k\sigma} = \sum_{n\sigma'} u_{n\sigma\sigma'}(\mathbf{k})\hat{\gamma}_{n\sigma'} + v^*_{n\sigma\sigma'}(\mathbf{k})\hat{\gamma}^\dagger_{n\sigma'}$, where $u_{n\sigma\sigma'}(\mathbf{k})$ and $v_{n\sigma\sigma'}(\mathbf{k})$ are quasi-particle and quasi-hole amplitudes respectively and $\hat{\gamma}_{n\sigma'}$ is a fermionic operator.

The mean-field pairing amplitude $\Delta = -U < c_{k\uparrow}c_{-k\downarrow} >$, where U is the pairwise attractive interaction potential, is obtained via the Bogoliubov amplitudes $u_{n\sigma}(\mathbf{k})$ and $v_{n\sigma}(\mathbf{k})$ (σ', being a pseudo-index, is omitted for simplicity) as

$$\begin{aligned}\Delta(\mathbf{k}) = -U\sum_n [u_{n\uparrow}(\mathbf{k})v^*_{n\downarrow}(-\mathbf{k})(1-f(E_n)) \\ + u_{n\downarrow}(\mathbf{k})v^*_{n\uparrow}(-\mathbf{k})f(E_n)]\end{aligned} \tag{S51}$$

where $f(x) = 1/(1+e^{x/(k_BT)})$ is the Fermi function at temperature T and k_B is the Boltzmann constant.

F. Self-consistent BdG formalism in real space

The conventional route to studying disordered superconductivity is to solve the self-consistent BdG equations $\mathcal{H}\phi_n(r_i) = \epsilon_n\phi_n(r_i)$ where $\phi_n = [u_{n\uparrow}(r_i), u_{n\downarrow}(r_i), v_{n\uparrow}(r_i), v_{n\downarrow}(r_i)]$ at every site using Bogoliubov transformation $\hat{c}_{i\sigma}(r_i) = \sum_{i,\sigma'} u_{n\sigma\sigma'}(r_i)\hat{\gamma}_{n\sigma'} + v^*_{n\sigma\sigma'}(r_i)\hat{\gamma}^\dagger_{n\sigma'}$. As above, the mean field pairing amplitude $\Delta(r_i) = -U < c_{i\uparrow}c_{i\downarrow} >$ and magnetization $m(r_i) =< c^\dagger_{i\uparrow}c_{i\uparrow} - c^\dagger_{i\downarrow}c_{i\downarrow} >$ are calculated from the following relations:

$$\begin{aligned}\Delta(r_i) = -U\sum_n [u_{n\uparrow}(r_i)v^*_{n\downarrow}(r_i)(1-f(E_n)) \\ + u_{n\downarrow}(r_i)v^*_{n\uparrow}(r_i)f(E_n)]\end{aligned} \tag{S52}$$

$$m(r_i) = \sum_{n,\sigma} u^*_{n\uparrow}u_{n\downarrow}f(E_n) + v_{n\uparrow}v^*_{n\downarrow}(1-f(E_n)) \tag{S53}$$

where $f(x) = 1/(1+e^{x/(k_BT)})$ is the Fermi function at temperature T and k_B is the Boltzmann constant.

G. Hamiltonian for Magnetic Impurity

The interaction between the magnetic impurity and the itinerant electrons can be represented by the Hund's coupling-like term $\hat{H}_{mag} = -J_H\sum_j \vec{S}_j \cdot \vec{s}_j$, where $\vec{S}_j$ is the impurity spin and $\vec{s}_j = \frac{1}{2}c^\dagger_{j\sigma}\vec{\sigma}_{\sigma\sigma'}c_{j\sigma'}$ represents the intrinsic electron spin. Assuming the impurity is represented by a classical spin of unit amplitude and polar angles θ and ϕ, the mean-field $\hat{H}_{mag}$ is

$$\hat{H}_{mag} = -\frac{J_H}{2}\begin{pmatrix} c^\dagger_{j\uparrow} & c^\dagger_{j\downarrow}\end{pmatrix}\Pi\begin{pmatrix} c_{j\uparrow} \\ c_{j\downarrow}\end{pmatrix} \tag{S54}$$

where,

$$\Pi = \begin{pmatrix} \cos\theta & \sin\theta\cos\phi - i\sin\theta\sin\phi \\ \sin\theta\cos\phi + i\sin\theta\sin\phi & -\cos\theta\end{pmatrix}$$

If we assume that the impurity spin is aligned perpendicular to the 2D-plane (*i.e.*, $\theta = 0$), we obtain

$\hat{H}_{mag} = -J_H/2 \sum_{j,\sigma,\sigma'} \boldsymbol{\sigma}^z_{\sigma\sigma'} c^\dagger_{j\sigma} c_{j\sigma'}$, where j runs over N_d number of impurity sites, randomly located in the two-dimensional space.

* nmohanta@phy.iitkgp.ernet.in
† slal@iiserkol.ac.in

[S1] Volovik, G. E. *The Universe in a Helium Droplet* (Oxford Univ. Press, Oxford, 2003).

[S2] Kramers, H. A. Théorie générale de la rotation paramagnétique dan le cristaux. *Proc. Amsterdam Acad.* **33**, 959 (1930); Sakurai, J. J. *Modern Quantum Mechanics* (Addison-Wesley, Reading, MA, 1994).

[S3] Sinova, J. *et al.* Universal Intrinsic Spin Hall Effect. *Phys. Rev. Lett.* **92**, 126603 (2004).

[S4] Kane, C. L. and Mele, E. J. Z_2 Topological Order and the Quantum Spin Hall Effect. *Phys. Rev. Lett.* **95**, 146802 (2005).

[S5] Senthil, T. and Fisher, M. P. A. Competing orders, nonlinear sigma models, and topological terms in quantum magnets. *Phys. Rev. B* **74**, 064405 (2006).

[S6] Abanov, A. G. and Wiegmann, P. B. Theta-terms in nonlinear sigma-models. *Nucl. Phys. B* **570**, 685 (2000).

[S7] Xu, C. and Ludwig, A. W. W. Nonperturbative Effects of a Topological Theta Term on Principal Chiral Nonlinear Sigma Models in $2+1$ Dimensions. *Phys. Rev. Lett.* **110**, 200405 (2013).

[S8] Lifshitz, I. M., Anomalies of electron characteristics of a metal in the high pressure region. *Sov. Phys. JETP* **11**, 1130-1135 (1960).

[S9] Rajaraman, R. *Solitons and Instantons: An Introduction to Solitons and Instantons in Quantum Field Theory* (North Holland Personal Library, Amsterdam, 1987).

[S10] Shankar, R. and Read, N. The $\Theta = \pi$ nonlinear sigma model is massless. *Nucl. Phys. B* **336**, 457 (1990); Controzzi, D. and Mussardo, G. Mass Spectrum of the Two-Dimensional $O(3)$ Sigma Model with a Θ Term. *Phys. Rev. Lett.* **92**, 021601 (2004).

[S11] Fradkin, E. *Field Theories of Condensed Matter Physics* (2nd Edition, Cambridge Univ. Press, Cambridge, 2013).

[S12] Witten, E. Nonabelian Bosonization in Two-Dimensions. *Commun. Math. Phys.* **92**, 455 (1984).

[S13] Knizhnik, V. G. and Zamolodchikov, A. B. Current Algebra and Wess-Zumino Model in Two-Dimensions. *Nucl. Phys. B* **247**, 83 (1984).

[S14] Lieb, E., Schultz, T. and Mattis, D. C. Two Soluble Models of an Antiferromagnetic Chain. *Ann. Phys. (N.Y.)* **16**, 407 (1961).

[S15] Nakamura, M. and Voit, J. Lattice twist operators and vertex operators in sine-Gordon theory in one dimension. *Phys. Rev. B* **65**, 153110 (2002)

[S16] Giamarchi, T. *Quantum Physics in One Dimension* (Oxford Univ. Press, Oxford, 2003).

[S17] Xu, C. and Moore, J. E. Stability of the quantum spin Hall effect: Effects of interactions, disorder, and Z_2 topology. *Phys. Rev. B* **73**, 045322 (2006).

[S18] Wu, C., Bernevig, A. and Zhang, S.-C. Helical Liquid and the Edge of Quantum Spin Hall Systems. *Phys. Rev. Lett.* **96**, 106401 (2006).

[S19] Mermin, N. D. and Wagner, H. Absence of Ferromagnetism or Antiferromagnetism in One- or Two-Dimensional Isotropic Heisenberg Models. *Phys. Rev. Lett.* **17**, 1133 (1966); Hohenberg, P. C. Existence of Long-Range Order in One and Two Dimensions. *Phys. Rev.* **158**, 383 (1967).

[S20] Affleck, I. Mass Generation by Merons in Quantum Spin Chains and the $O(3)$ σ Model. *Phys. Rev. Lett.* **56**, 408 (1986); *ibid.*, Quantum spin chains and the Haldane gap. *J. Phys. Cond. Matt.* **1**, 3047 (1989).

[S21] Tanaka, A., Totsuka, K. and Hu, X. Geometric phases and the magnetization process in quantum antiferromagnets. *Phys. Rev. B* **79**, 064412 (2009).

[S22] Berezinskii, V. L. Destruction of long-range order in one-dimensional systems having a continuous symmetry group I. Classical systems. *Sov. Phys. JETP* **32**, 493 (1971); Kosterlitz, J. M. and Thouless, D. J. Ordering, metastability and phase transitions in two-dimensional systems. *J. Phys. C* **6**, 1181 (1973).

[S23] Horowitz, B., Bohr, T., Kosterlitz, J. M. and Schulz, H. J. Commensurate-incommensurate transitions and a floating devil's staircase. *Phys. Rev. B* **28**, 6596 (1983).

[S24] Wen, X. G. Chiral Luttinger liquid and the edge excitations in the fractional quantum Hall states. *Phys. Rev. B* **41**, 12838 (1990); *ibid.*, Gapless boundary excitations in the quantum Hall states and in the chiral spin states. *Phys. Rev. B* **43**, 11025 (1991); *ibid.*, Edge transport properties of the fractional quantum Hall states and weak-impurity scattering of a one-dimensional charge-density wave. *Phys. Rev. B* **44**, 5708 (1991).

[S25] Lal, S., Rao, S. and Sen, D. Conductance through contact barriers of a finite-length quantum wire. *Phys. Rev. B* **65**, 195304 (2002).

[S26] Polyakov, A. M. Interaction of goldstone particles in two dimensions. Applications to ferromagnets and massive Yang-Mills fields. *Phys. Lett. B* **59**, 79 (1975).

[S27] Haldane, F. D. M. Continuum dynamics of the 1-D Heisenberg antiferromagnet: Identification with the $O(3)$ nonlinear sigma model. *Phys. Lett. A* **93**, 464 (1983); *ibid.*, Nonlinear Field Theory of Large-Spin Heisenberg Antiferromagnets: Semiclassically Quantized Solitons of the One-Dimensional Easy-Axis Néel State. *Phys. Rev. Lett.* **50**, 1153 (1983); Affleck, I. and Haldane, F. D. M. Critical theory of quantum spin chains. *Phys. Rev. B* **36**, 5291 (1987).

[S28] Affleck, I. Exact critical exponents for quantum spin chains, non-linear σ models at $\theta = \pi$ and the quantum Hall effect. *Nucl. Phys. B* **265**, 409 (1986).

[S29] Sen, D. and Lal, S. One-dimensional fermions with incommensuration. *Phys. Rev. B* **61**, 9001 (2000); Tanaka, A. and Hu, X. Effective field theory with a θ-vacua structure for two-dimensional spin systems. *Phys. Rev. B* **74**, 140407 (R) (2006).

[S30] Goldenfeld, N. *Lectures on Phase Transitions and the Renormalization Group*, (Addison-Wesley, 1992).